AFRL-AFOSR-VA-TR-2021-0013

High-Speed, Real-Time Infrared Imaging of Hot Spots in Reactive Materials: Dynamic Experiments and 3D Modeling

Guduru, Pradeep
BROWN UNIVERSITY
230 W 41ST STREET FL 7
NEW YORK, NY, 02912-9100
US

02/05/2021
Final Technical Report

Air Force Research Laboratory
Air Force Office of Scientific Research
Arlington, Virginia 22203
Air Force Materiel Command

REPORT DOCUMENTATION PAGE

Form Approved
OMB No. 0704-0188

1. REPORT DATE *(DD-MM-YYYY)*	**2. REPORT TYPE**	**3. DATES COVERED** *(From - To)*
05-02-2021	Final	30 Sep 2015 - 29 Mar 2020

4. TITLE AND SUBTITLE
High-Speed, Real-Time Infrared Imaging of Hot Spots in Reactive Materials: Dynamic Experiments and 3D Modeling

5a. CONTRACT NUMBER

5b. GRANT NUMBER
FA9550-15-1-0415

5c. PROGRAM ELEMENT NUMBER

6. AUTHOR(S)
Pradeep Guduru

5d. PROJECT NUMBER

5e. TASK NUMBER

5f. WORK UNIT NUMBER

7. PERFORMING ORGANIZATION NAME(S) AND ADDRESS(ES)
BROWN UNIVERSITY
230 W 41ST STREET FL 7
NEW YORK, NY 02912-9100
US

8. PERFORMING ORGANIZATION REPORT NUMBER

9. SPONSORING/MONITORING AGENCY NAME(S) AND ADDRESS(ES)
AF Office of Scientific Research
875 N. Randolph St. Room 3112
Arlington, VA 22203

10. SPONSOR/MONITOR'S ACRONYM(S)
AFRL/AFOSR RTA1

11. SPONSOR/MONITOR'S REPORT NUMBER(S)
AFRL-AFOSR-VA-TR-2021-0013

12. DISTRIBUTION/AVAILABILITY STATEMENT
A Distribution Unlimited: PB Public Release

13. SUPPLEMENTARY NOTES

14. ABSTRACT
This project consists of two components: (i) design and development of a high speed infrared imaging system and (ii) pressure-shear plate impact experiments on energetic materials (or their simulants). The eventual objective is to combine (i) and (ii) to visualize hot spot evolution in energetic materials under well-defined plane wave loading conditions. Under task (i),
we have designed and built a unique high speed infrared imaging system to image temperature fields associated with hotspot evolution in energetic materials under high rate deformation. The system consists of a 24x24 array of HgCdTe detectors that constitutes the focal plane array. We have designed a fan-out chip that provides individual access to each pixel, a flexible
printed circuit board to carry the signals to outside the dewar for signal processing, custom optics for diffraction limited imaging and a high speed data-acquisition to acquire images at up to a million frames per second. The progress report on the status of this effort is reported separately. Pressure-shear plate impact (PSPI) experiments were conducted to study the mechanical behavior of HTPB binder and sucrose (energetic material simulant) at high strain rates and high pressures. The main finding of these experiments is that, although HTPB is a soft elastomer at ambient conditions, its shear strength can be as high as 0.5 GPa under a pressure of about 9 GPa and a strain rate of 0.4 x 106 1/s. At similar pressures and shearing rates, PSPI experiments on sucrose — a simulant for energetic crystals — show a shearing resistance of 288 MPa. In these
experiments, sucrose exhibits pronounced strain softening, even a dramatic drop in shearing resistance at large shear strains. Pressure-shear plate impact experiments have also been conducted on HTPB-sucrose composite specimens as well. We have carried out a detailed constitutive modeling of HTPB and sucrose so the observed material behavior can be
incorporated into computational modeling in order to capture realistic response under extreme loading conditions. Ongoing work includes implementing these constitutive models to simulate the experimental results on the composite specimens.

15. SUBJECT TERMS

16. SECURITY CLASSIFICATION OF:			**17. LIMITATION OF ABSTRACT**	**18. NUMBER OF PAGES**	**19a. NAME OF RESPONSIBLE PERSON**
a. REPORT	**b. ABSTRACT**	**c. THIS PAGE**			MARTIN SCHMIDT
U	U	U	UU	46	**19b. TELEPHONE NUMBER** *(Include area code)* 588-8436

Grant#FA9550-15-1-0415
High-Speed, Real-Time Infrared Imaging of Hot Spots in Reactive Materials: Dynamic Experiments and 3D Modeling

Dynamic Shearing Resistance of HTPB, Sucrose and HTPB-Sucrose Composite Material

Pinkesh Malhotra, Tong Jiao, Rodney J. Clifton and Pradeep Guduru*

School of Engineering, Brown University
*pradeep_guduru@brown.edu

Abstract. This project consists of two components: (i) design and development of a high speed infrared imaging system and (ii) pressure-shear plate impact experiments on energetic materials (or their simulants). The eventual objective is to combine (i) and (ii) to visualize hot spot evolution in energetic materials under well-defined plane wave loading conditions. Main accomplishments on the above two tasks are summarized below.

Under task (i), we have designed and built a unique high speed infrared imaging system to image temperature fields associated with hot-spot evolution in energetic materials under high rate deformation. The system consists of a 24x24 array of HgCdTe detectors that constitutes the focal plane array. We have designed a fan-out chip that provides individual access to each pixel, a flexible printed circuit board to carry the signals to outside the dewar for signal processing, custom optics for diffraction limited imaging and a high speed data-acquisition to acquire images at up to a million frames per second. The progress report on the status of this effort is presented under the associated DURIP grant # FA9550-15-1-0451.

As part of task (ii), pressure-shear plate impact (PSPI) experiments were conducted to study the mechanical behavior of HTPB binder and sucrose (energetic material simulant) at high strain rates and high pressures. The main finding of these experiments is that, although HTPB is a soft elastomer at ambient conditions, its shear strength can be as high as 0.5 GPa under a pressure of about 9 GPa and a strain rate of 0.4 x 106 1/s. At similar pressures and shearing rates, PSPI experiments on sucrose — a simulant for energetic crystals — show a shearing resistance of 288 MPa. In these experiments, sucrose exhibits pronounced strain softening, even a dramatic drop in shearing resistance at large shear strains. Pressure-shear plate impact experiments have also been conducted on HTPB-sucrose composite specimens as well.

We have carried out a detailed constitutive modeling of HTPB and sucrose so the observed material behavior can be incorporated into computational modeling in order to capture realistic response under extreme loading conditions. Ongoing work includes implementing these constitutive models to simulate the experimental results on the composite specimens.

1. Introduction: Polymer-bonded explosives (PBXs) are composites of energetic crystals held together by a polymeric binder. It is essential to predict their high-pressure, high-strain rate response in order to be able to understand the mechanisms of hot spot formation and how they are influenced by the microstructure. Here, we employed one-dimensional plane wave experiments to

Component	Chemical used	% by weight
Pre-polymer	Hydroxyl-terminated polybutadiene (HTPB)	47.380
Plasticizer	Dioctyl adipate (DOA)	47.300
Anti-oxidant	2,2'-methylene-bis-(4-methyl-tert-butylphenol (AO-2246)	0.635
Catalyst	Dibutyltin dilaurate (DBTDL)	0.095
Curing Agent	Isophorone diisocyanate (IPDI)	4.632

TABLE 1. Binder Composition

measure the mechanical response of hydroxyl-terminated butadiene (HTPB) and sucrose. HTPB is a commonly used elastomeric binder in PBXs. The compressive behavior of HTPB has been characterized in the past studies at a range of strain rates (10^{-3} to 10^{6} s^{-1}) [1,2,3,4]. However, the shearing resistance at high shearing rates and high pressures has not been established. Shearing resistance under such conditions is important because of its connection with localization, hot spots, and phase transformations. Similarities between shock Hugoniots of granulated sucrose and HMX have been shown by [5] and [6], using plate impact experiments. Sucrose has been demonstrated to show deformation behavior similar to that of HMX and RDX under drop-weight loading [7]. These experiments, along with the similarity of sucrose's monoclinic crystal structure, further support the choice of sucrose as a simulant for HMX. While previous studies focused on compression behavior of a granulated form of sucrose, our studies herein examined the shearing resistance of a thin, nominally uniform, layer of sucrose under high pressures and shear strain-rates.

2. PSPI Experiments on HTPB, Sucrose and HTPB-Sucrose Composite: PSPI experiments were employed to investigate the mechanical behavior of HTPB and sucrose. In these experiments, the sample is sandwiched between two hard elastic plates, usually made from pure tungsten carbide. The sandwich is impacted by a hard elastic flyer at an angle θ. A combined Normal Displacement Interferometer (NDI) and Transverse Displacement Interferometer (TDI) is used to

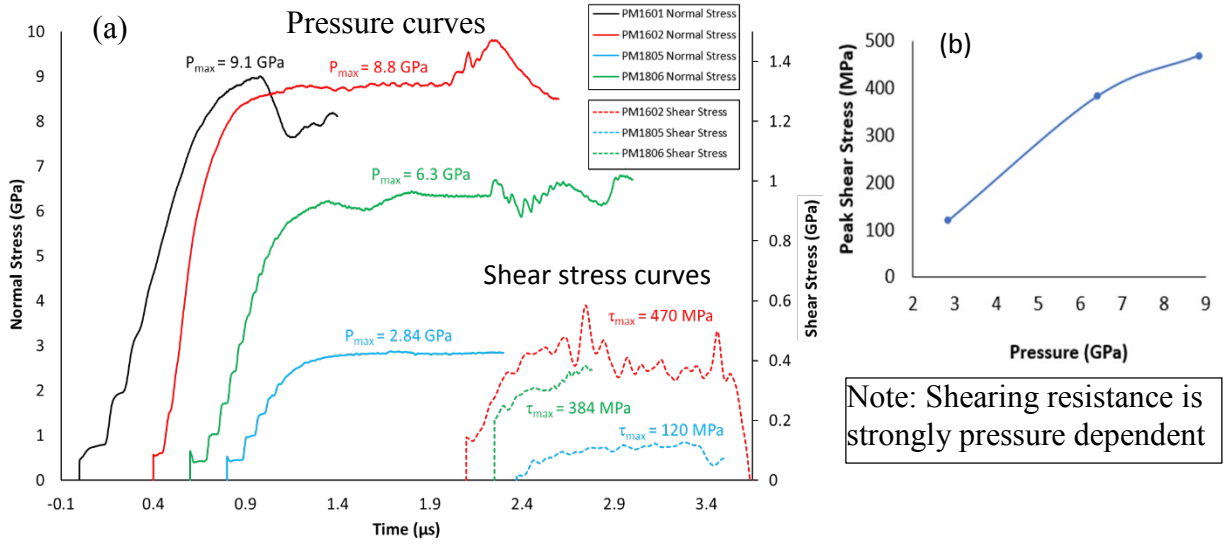

Figure 1. (a) Results of the pressure shear plate impact experiments on HTPB binder. The pressures are varied between 2.8 and 9 GPa. (b) The corresponding shear resistance varies between 120 MPa and 470 MPa, displaying a strong pressure dependence.

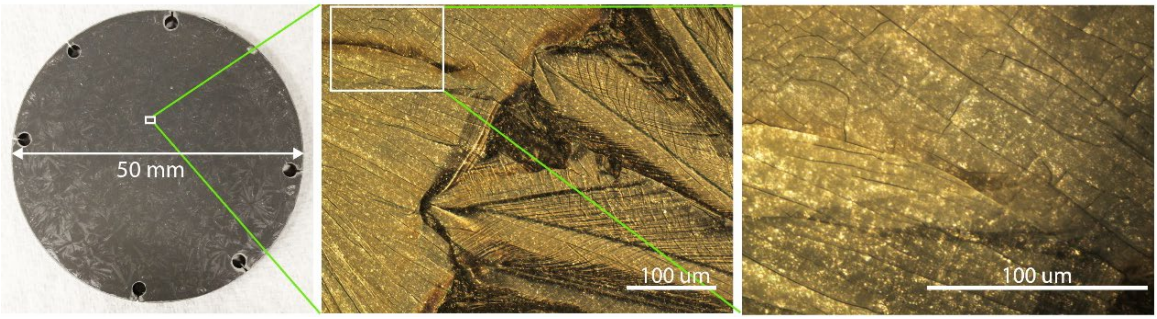

Figure 2. Spin-coated sucrose on WC (left) showing cracks (right) after cooling down.

measure rear surface velocities (more details by Clifton and Klopp [8]). Velocities and tractions at the sample/rear-plate interface are inferred from the measured rear surface velocities, using 1D elastic wave analysis.

The composition of HTPB studied here is given in Table 1. This composition is the same as that reported in [9], except that no bonding agent is used. Stiffness of the binder can be changed easily by changing the relative fractions of the plasticizer [1] or the curing agent or both. NCO:OH=1:1 is used in the present study. The components are mixed, followed by degassing down to ~3 kPa. The degassed mixture is then cast between the target plates and cured at 60 ^{0}C for one day. Figure 1 shows a summary of the results of the pressure-shear plate impact experiments in which the pressure is varied between 2.8 GPa and about 9 GPa. The significant result is that the corresponding shearing resistance varies between 120 MPa and 470 MPa, revealing a strong pressure dependence. Further, note that, under ambient conditions, HTPB is rubbery, with a shear strength of no more than a few MPa. Thus, it is essential to incorporate the measured pressure dependence of the strength of HTPB in computational simulations.

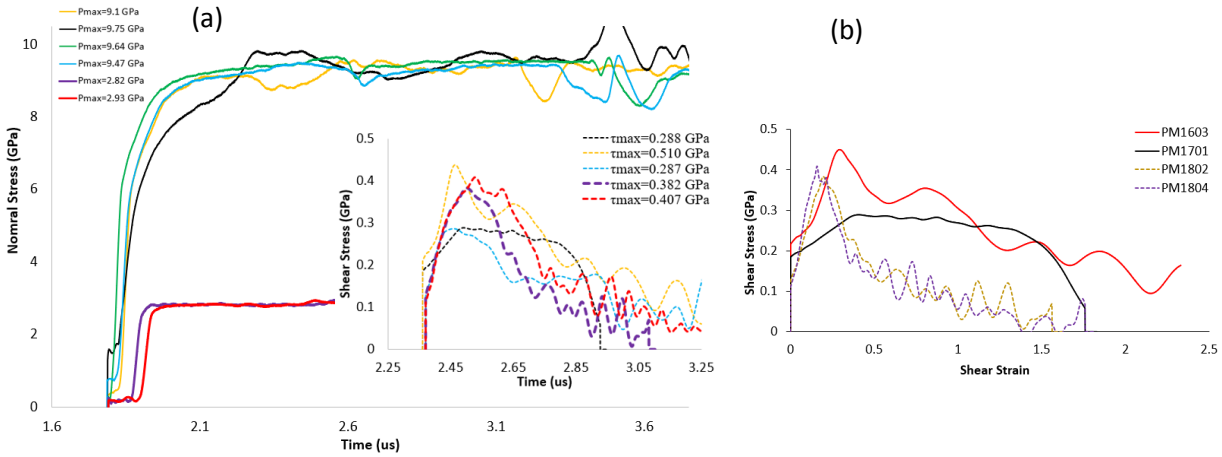

Figure 3. (a) Results of the pressure shear plate impact experiments on crystalline sucrose. Two pressures are used: approximately 3 GPa and 9.5 GPa. The shear stress response has two distinct features: it is relatively insensitive to the pressure; it shows localization-like behavior, with the shear strength dropping progressively with accumulated shear strain. (b) Loss of shear strength with shear strain; note the large magnitude of the imposed strains. Further note that, at a pressure of about 9GPa, the shear strength of the HTPB binder is comparable to that of sucrose!

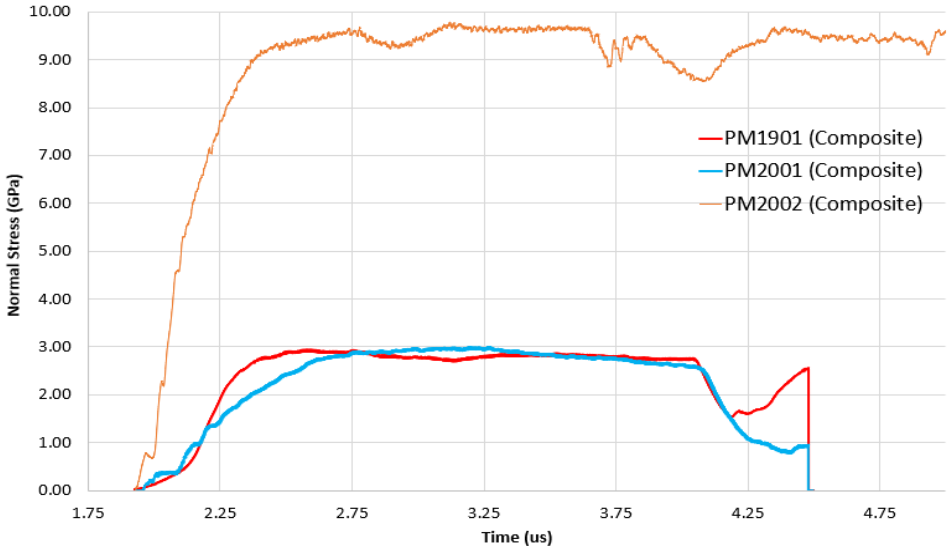

Figure 4. Normal pressure vs. time evolution for HTPB-Sucrose composites shots. Note that two normal stress values are employed, i.e., ~3 GPa and ~9.5GPa.

Spin-coating is used to prepare a thin, uniform layer of sucrose. An 80 wt% sucrose solution, in water, is prepared and degassed to remove bubbles. The solution is spin-coated onto the front target plate at 4000 rpm, followed by drying at 55 ^{0}C for 12-16 hours until all the water has evaporated. This procedure yields a thickness of about 17 microns, with surface roughness (Ra~2.5 µm) and fine cracks resulting from differences in thermal expansion of sucrose and WC (Figure 2). It is important to choose the initial concentration in the labile zone, above the meta-stability limit, corresponding to the drying temperature used. A concentration lower than the meta-stability limit would lead to no nucleation and hence no-grains. On the other hand, a concentration above the glass-transition curve will lead to an undesired amorphous layer. Relative Humidity of the drying environment also plays a critical role in the evaporation process and in the formation of a crystalline layer on the WC. The crystallinity of the spin-coated layer is confirmed by comparison of X-ray diffraction patterns with those of crystalline sucrose powder.

Figure 3 shows a summary of the pressure shear plate impact experiments on sucrose films. Two pressure values are imposed: one around 3 GPa and the other around 9.5 GPa. The shear stress response has two distinct features: it is relatively insensitive to the pressure; it shows localization-like behavior, with the shear strength dropping progressively with accumulated shear strain. Note that the imposed shear strains are quite large, up to 2. Further note that, at a pressure of about 9 GPa, the shear strength of the HTPB binder is comparable to that of sucrose! In other words, the binder, which nominally very soft and rubbery under ambient conditions, is as strong as sucrose at high pressures. Such response has significant influence on energy dissipation and localization mechanisms.

Further, dropping shear strength of sucrose with accumulated shear strain indicates a tendency to localize, possibly through adiabatic shear band formation. The implication is that such a localization mechanism in the energetic crystal is a possible hot spot mechanism that needs to be investigated in isolation.

Sucrose-HTPB composite samples were prepared with 90% (weight) of sucrose, with grain sizes in the range of ~50-100 μm. PSPI experiments were conducted with two values of normal pressures: ~3 GPa and ~9.5 GPa. A summary of the normal and shear responses is shown in Figures

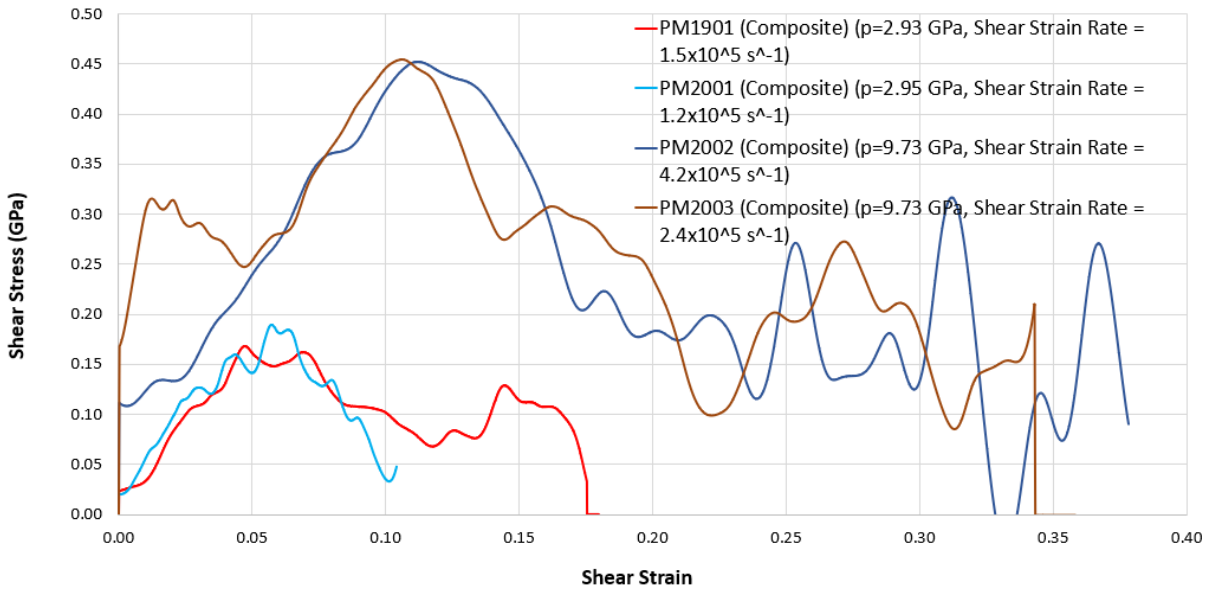

Figure 5. Shear stress vs. time evolution for HTPB-Sucrose composites shots. Note the drop in shear strength, which is characteristic of the sucrose behavior, suggesting possible localization in sucrose.

4 and 5 respectively. It is worth noting that the shear strength of the composite displays drop is strength, suggesting localization, either in the HTPB binder or in sucrose crystals.

3. Constitutive modeling of HTPB binder: a quasi-viscoelastic model

Model Description: The basic idea is to model the stress response as (a) instantaneous elastic response followed by (b) relaxation with a continuous distribution of effective relaxation times. The model includes pressure dependence of shear wave speed. For the instantaneous elastic response, we employ a multiplicative decomposition of strain energy density as follows

$$\bar{W}(J,\bar{I}_1,\bar{I}_2) = f(J)\,\hat{W}(\bar{I}_1,\bar{I}_2) = f(J)C_{00} + f(J)\big(C_{10}(\bar{I}_1-3) + C_{01}(\bar{I}_2-3)\big)$$

which incorporates pressure dependence, which is typically ignored in quasi-static polymer modeling. A Lennard-Jones like dependence is used:

$$f(J) = (J^{-M} - 2J^{-N}) + 2$$

Where $N = M/2$. Distortional strain energy is taken to be of the form of Mooney-Rivlin:

$$\hat{W}(\bar{I}_1,\bar{I}_2) = C_{00} + C_{10}(\bar{I}_1-3) + C_{01}(\bar{I}_2-3)$$

Where

$$\bar{I}_1 = \frac{I_1}{J^{\frac{2}{3}}} = \frac{1}{J^{\frac{2}{3}}}\,tr\boldsymbol{B}$$

$$\bar{I}_2 = \frac{I_2}{J^{\frac{4}{3}}} = \frac{1}{J^{\frac{4}{3}}}\frac{[(tr\boldsymbol{B})^2 - tr\boldsymbol{B}^2]}{2}$$

$$J = det\boldsymbol{F}$$

The Cauchy Stress is obtained from the 2nd Piola Kirchoff (PK)stress as:

$$\boldsymbol{T} = \frac{2}{J^{5/3}}\left(\frac{\partial \bar{W}}{\partial \bar{I}_1} + \bar{I}_1\frac{\partial \bar{W}}{\partial \bar{I}_2}\right)\boldsymbol{B} - \left(\frac{2}{J^{\frac{7}{3}}}\frac{\partial \bar{W}}{\partial \bar{I}_2}\right)\boldsymbol{B}^2 + \frac{1}{J}\left(-\frac{2}{3}\bar{I}_1\frac{\partial \bar{W}}{\partial \bar{I}_1} - \frac{4\bar{I}_2}{3}\frac{\partial \bar{W}}{\partial \bar{I}_2} + J\frac{\partial \bar{W}}{\partial J}\right)\boldsymbol{I}$$

The material parameters (C_{00}, C_{10}, C_{01}) that describe instantaneous elastic response are determined from the elastic wave speeds as described in a subsequent section.

For linear viscoelasticity, the relaxed stress is related to instantaneous stress as:

$$\bar{\sigma}(t) = \sigma^e(t) + \int_0^t \sigma^e(t-t')\,\frac{dR(t')}{dt'}\,dt'$$

For a standard linear solid, the relaxation function is given as:

$$R(t) \equiv \frac{E(t)}{E(0)} = \frac{E_\infty}{E_0} + \left(1 - \frac{E_\infty}{E_0}\right)e^{-\frac{t}{t_R}} = \zeta + (1-\zeta)e^{-\frac{t}{t_R}}$$

Where $\zeta = \frac{E_\infty}{E_0} < 1$ is the ratio of rubbery and glassy moduli. Instead of having one relaxation time, t_R, assume a continuous distribution of times $S(t_R)$. Therefore, the relaxation function now is:

$$R(t) = \int_0^\infty \left(\zeta + (1-\zeta)e^{-\frac{t}{t_R}}\right)S(t_R)\,dt_R$$

Since $R(0) = 1$, $\int_0^\infty S(t_R)dt_R = 1$.

Using some physical arguments, it can be shown that the distribution of relaxation times $S(t_R)$ can be obtained as:

$$S(t_R) = \begin{cases} S_0 & t_1 < t_R < t_2 \\ 0 & otherwise \end{cases}$$

Since $\int_0^\infty S(t_R)dt_R = 1$, $S_0 = \frac{1}{t_2 - t_1}$. Using the above distribution, the relaxation function is simplified as:

$$R(t) = \zeta + \left(\frac{1-\zeta}{t_2 - t_1}\right)\int_{t_1}^{t_2} e^{-t/t_R}\,dt_R$$

$$\frac{dR}{dt}(t) = \left(\frac{1-\zeta}{t_2 - t_1}\right)\int_{1/t_1}^{1/t_2} e^{-tu}\frac{du}{u} = \left(\frac{1-\zeta}{t_2 - t_1}\right)\left(\ln\left(\frac{t_1}{t_2}\right) + \sum_{n=1}^{\infty}\frac{\left(-\frac{t}{t_2}\right)^n - \left(-\frac{t}{t_1}\right)^n}{n \times n!}\right)$$

The exponential integral can be approximated using the Swamee and Ohija approximation:

$$E_1(x) = \int_x^\infty \frac{e^{-t}}{t}dt \approx (A^{-7.7} + B)^{-0.13}$$

$$A = \ln\left[\left(\frac{0.56146}{x} + 0.65\right)(1+x)\right]$$

$$B = x^4 e^{7.7x}(2+x)^{3.7}$$

An alternative distribution of relaxation times that can be used is:

$$S(t_R) = \begin{cases} \frac{c}{t_R} & t_1 < t_R < t_2 \\ 0 & otherwise \end{cases}$$

In this distribution, the shorter time scales are weighed heavier than the larger time scales. The shorter scales are important in wave propagation problems. Cut-offs (t_1 and t_2) are placed keeping in mind the application of interest.

$$R(t) = \frac{1 + \int_0^\infty S(t')e^{-\frac{t}{t'}}dt'}{1 + \int_0^\infty S(t')dt'} = \frac{1 + \int_{t_1}^{t_2} S(t')e^{-\frac{t}{t'}}dt'}{1 + \int_{t_1}^{t_2} S(t')dt'}$$

$$= \begin{cases} 1 & t = 0 \\ \dfrac{1 + c\left[E_1\left(\frac{t}{t_2}\right) - E_1\left(\frac{t}{t_1}\right)\right]}{1 + c\ ln\left(\frac{t_2}{t_1}\right)} & t \geq 0 \end{cases}$$

Where $E_1(z) = \int_z^\infty \frac{e^{-t}}{t} dt$ is the exponential integral function.

$$\frac{dR}{dt}(t) = \begin{cases} \left[\dfrac{c}{1 + c\ ln\left(\frac{t_2}{t_1}\right)}\right]\left(\dfrac{1}{t_2} - \dfrac{1}{t_1}\right) & t = 0 \\ \left[\dfrac{c}{1 + c\ ln\left(\frac{t_2}{t_1}\right)}\right]\left(\dfrac{e^{-t/t_1} - e^{-t/t_2}}{t}\right) & t > 0 \end{cases}$$

Application to the PSPI experiments on HTPB

For the case of simple shear deformation imposed in the PSPI experiments, the instantaneous elastic response takes the following specific form:

$$F = \begin{pmatrix} \lambda & 0 & 0 \\ -\kappa & 1 & 0 \\ 0 & 0 & 1 \end{pmatrix}$$

$$\bar{W}(J, \bar{I}_1, \bar{I}_2) = f(J)\ \hat{W}(\bar{I}_1, \bar{I}_2)$$

$$f(J) = (J^{-M} - 2J^{-N}) + 2$$

$$\hat{W}(\bar{I}_1, \bar{I}_2) = C_{00} + C_{10}(\bar{I}_1 - 3) + C_{01}(\bar{I}_2 - 3)$$

Generally, the internal energy per unit mass is $U = U(\boldsymbol{E}, S)$. For the instantaneous elastic response, since the deformation is reversible, $U = U_e(\boldsymbol{E}, S_0) = U_e(\boldsymbol{E})$ where $\boldsymbol{E}$ is the Lagrangian strain. For an isotropic material, strain energy is a function of the invariants:

$$U_e(\boldsymbol{E}) = \frac{1}{\rho_0} W(I_1, I_2, I_3) = \frac{1}{\rho_0} \bar{W}(\bar{I}_1, \bar{I}_2, J)$$

The 2nd PK stress is given as:

$$\boldsymbol{S} = \rho_0 \frac{dU}{d\boldsymbol{E}} = \frac{d\bar{W}}{d\boldsymbol{E}}$$

And the Cauchy stress is given as:

$$\boldsymbol{T} = \frac{1}{J}\boldsymbol{F}\boldsymbol{S}\boldsymbol{F}^T$$

Simplifying the expression, this is given as:

$$\boldsymbol{T} = 2f(\lambda)\left[\frac{C_{10}}{\lambda^{5/3}} + \frac{C_{01}\bar{I}_1}{\lambda^{5/3}}\right]\boldsymbol{M_1} - \frac{2C_{01}}{\lambda^{\frac{7}{3}}}f(\lambda)\boldsymbol{M_2} + \left\{[C_{00} + C_{01}(\bar{I}_2 - 3) + C_{10}(\bar{I}_1 - 3)]f'(\lambda) - \frac{f(\lambda)}{\lambda}\left[\frac{2C_{10}\bar{I}_1}{3} + \frac{4C_{01}\bar{I}_2}{3}\right]\right\}\boldsymbol{I}$$

Where the matrices are defined as:

$$\boldsymbol{M_1} = \begin{pmatrix} \lambda^2 & -\kappa\lambda & 0 \\ -\kappa\lambda & \kappa^2 + 1 & 0 \\ 0 & 0 & 1 \end{pmatrix}$$

$$\boldsymbol{M_2} = \begin{pmatrix} \lambda^2(\lambda^2 + \kappa^2) & -\kappa\lambda(1 + \kappa^2 + \lambda^2) & 0 \\ -\kappa\lambda(1 + \kappa^2 + \lambda^2) & (1 + \kappa^2)^2 & 0 \\ 0 & 0 & 1 \end{pmatrix}$$

The invariants are:

$$\bar{I}_1 = \lambda^{\frac{4}{3}} + \kappa^2\lambda^{-\frac{2}{3}} + 2\lambda^{-\frac{2}{3}}$$
$$\bar{I}_2 = 2\lambda^{\frac{2}{3}} + \kappa^2\lambda^{-\frac{4}{3}} + \lambda^{-\frac{4}{3}}$$
$$J = \lambda$$

It can be found that (since $M = 2N$):

$$K = (M^2 - 2N^2)C_{00} = 2N^2C_{00}$$
$$\mu = 2(C_{01} + C_{10})$$

It is assumed that $C_{01} = C_{10} = \frac{\mu}{4}$. Therefore, Cauchy stress can be simplified as:

$$\boldsymbol{T} = \frac{2f(\lambda)C_{10}}{\lambda^{\frac{5}{3}}}(1 + \bar{I}_1)\boldsymbol{M_1} - \frac{2C_{10}}{\lambda^{\frac{7}{3}}}f(\lambda)\boldsymbol{M_2} + \left\{[C_{00} + C_{10}(\bar{I}_1 + \bar{I}_2 - 6)]f'(\lambda) - \frac{2f(\lambda)}{3\lambda}C_{10}(\bar{I}_1 + 2\bar{I}_2)\right\}\boldsymbol{I}$$

Finding λ and κ from $\boldsymbol{U}$:

$$\boldsymbol{C} = \boldsymbol{U}^2 = \boldsymbol{F}^T\boldsymbol{F} = \begin{pmatrix} \lambda^2 + \kappa^2 & -\kappa & 0 \\ -\kappa & 1 & 0 \\ 0 & 0 & 1 \end{pmatrix}$$

Relaxation Calculations: This relaxation function can be separately applied to the deviatoric and volumetric components of stress as they might relax in different ways. For example, the relaxed deviatoric stress components can be calculated as:

$$s_{ij}(t) = s_{ij}^e(t) + \int_0^t s_{ij}^e(t - u)\,\frac{dR(u)}{du}\,du$$

Evaluating the integral using the trapezoidal rule,

$$\int_a^b f(x)dx \approx \sum_{m=1}^{n} \frac{f(x_{m-1}) + f(x_m)}{2}\Delta x_m\,;(x_0 = a, x_n = b)$$

If $\Delta x_m = \Delta x = \frac{b-a}{n}$, $x_m = a + m\Delta x$.

Assume the time interval is given by Δt. At time t, number of time-intervals passed is $q = \frac{t}{\Delta t}$, assuming that time advances discretely in intervals of Δt. Our aim is to estimate $s_{ij}(t)$. Applying the trapezoidal rule, we get

$$s_{ij}(t) \approx s_{ij}^{e}(t) + \sum_{m=1}^{q} \frac{f(u_{m-1}) + f(u_m)}{2} \Delta u$$

$$b_d = \frac{c_d}{1 + c_d \ln\left(\frac{t_{d2}}{t_{d1}}\right)}$$

$$u_m = m\Delta u; t = q\Delta t$$

$$f(u_m) = s_{ij}^{e}(t - u_m)\frac{dR}{du}(u_m) \xrightarrow{Shorthand} s_{ij}^{e}(q - m)\frac{dR}{du}(m)$$

Note that due to change in variables inside the integral, the time increment now becomes Δu instead of Δt. The subscript 'd' indicates 'deviatoric'. Three variables of interest here are: t_1, t_2, c. The above model is implemented through a VUMAT in ABAQUS in order to obtain the best fit values for the model parameters.

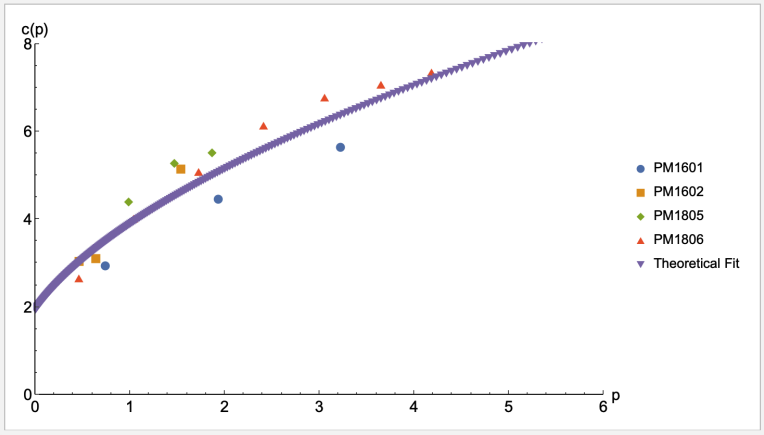

Figure 6. Wave speed vs. pressure obtained from the normal response in the PSPI experiments. Symbols indicate the experimental data and the solid line is the model fit.

QUASI-ISENTROPE ANALYSIS: FINDING WAVE SPEED AS A FUNCTION OF NORMAL STRESS

The wave speeds are calculated using a Lennard-Jones potential:

$$U_{LJ} = B(J^{-M} - 2J^{-N})$$

Pressure can be found from the potential using:

$$p(J) = -\rho_0 \frac{dU_{LJ}}{dJ} = \rho_0 BM(J^{-M-1} - J^{-N-1}) = A(J^{-M-1} - J^{-N-1})$$

$$assuming\ M = 2N$$

The longitudinal wave speed can be found using:

$$c(J) = \sqrt{\frac{1}{\rho_0}\frac{dp}{d\epsilon}} \xrightarrow{J=1+\epsilon} \sqrt{-\frac{A}{\rho_0}\left[(M+1)J^{-M-2} - (N+1)J^{-N-2}\right]}$$

From these equations, we have $p(J)$ and $c(J)$. We wish to plot $p(J) vs\ c(J)$ or find $c(p)$. However, finding an explicit expression from the above equations is very hard. Since the values of A and J serve only as a starting point in the ABAQUS simulations, it is not necessary to have an optimal value from the quasi-isentrope analysis. Therefore, a good fit is gauged without a strict quality measure and plotted in Figure 6, along with the experimental data. Reasonable agreement is found for $M = 6$ and $A = 1.25 \times 10^9$.

The parameters for the quasi-linear viscoelastic model to describe the shear stress response are obtained by fitting the experimental data. The strategy is to obtain the best fit parameters from one experiment and verify them by predicting the response for the remaining experiments. Figures 7 shows the fit to obtain the parameters and Figures 8 shows the predicted response for a different experiment. Note that the model performs remarkably well.

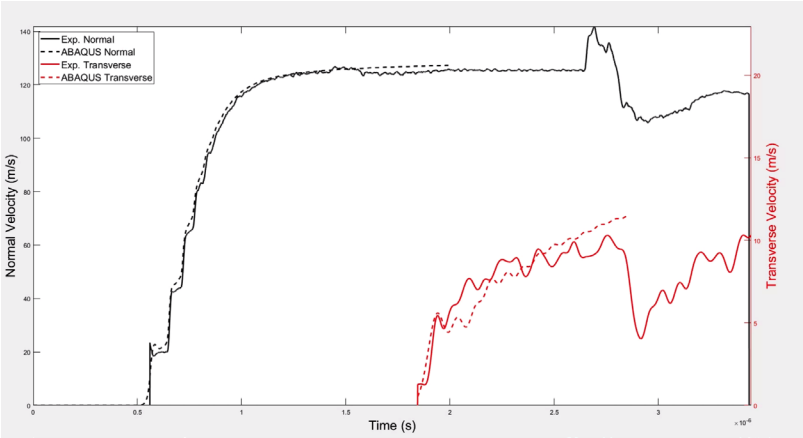

Figure 7. Extraction of the parameters by fitting the model predictions with one of the PSPI experiments. The solid lines are experimental data and the dashed lines are model fits.

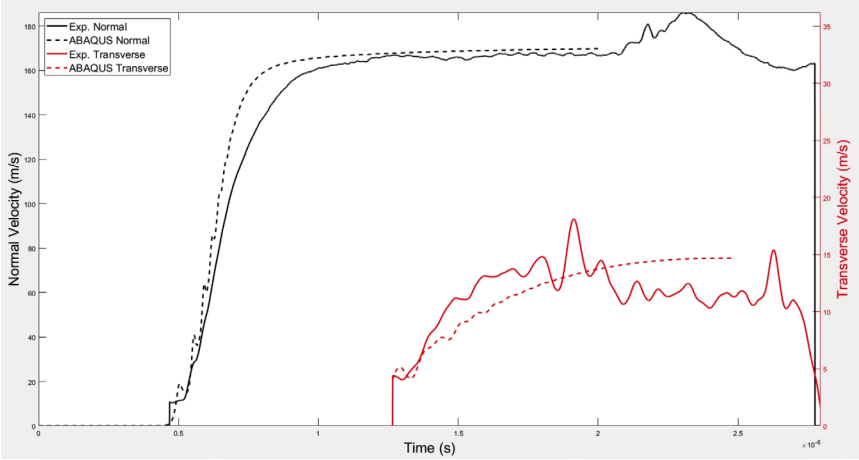

Figure 8. Comparison of the model predictions and the experimental data. The model parameters are those extracted from a different shot shown in Fig. 7. The solid lines are experimental data and the dashed lines are model fits.

4. Constitutive Modeling of Sucrose

Energetic crystals like HMX, RDX and PETN and their simulant crystals like sucrose are in general complex molecular solids, characterized by anisotropic crystal structures and complex molecular arrangements. As a result, the response of such molecular solids to mechanical loading is inherently complex. However, in order to accurately model material response and capture the physics behind phenomena like pore collapse and subsequent chemical reactions, it is imperative to retain maximum features of a most generalized model albeit at the expense of complexity and computational resources expended. A general material model for such molecular solids should incorporate: (a) a finite deformation framework, (b) non-linear anisotropic thermo-elasticity, i.e. have anisotropic elastic moduli which are dependent on pressure and temperature in general, and the ability to handle finite non-linear elastic deformations under large pressures through a complete equation of state, (c) plastic anisotropy, typically modeled using the crystal plasticity approach, and (d) thermo-elastic heat generation and plastic dissipation. This section focuses on creating a thermodynamically consistent framework for finite deformation modeling of sucrose. The framework presented here is generic and can be used for any isotropic material subject to extreme dynamic environments involving high pressures, large strain-rates and strains, both in compressive and shear loading scenarios.

THERMODYNAMICS OF A SOLID

Kinematics

Consider a body occupying a region of space, $\mathcal{B}_0$ in the reference/undeformed configuration. The body is then subjected to a motion, $\boldsymbol{x} = \boldsymbol{\chi}(\boldsymbol{X}, t)$ so that it now occupies a region of space, $\mathcal{B}_t$ at time t in the spatial/deformed configuration. The deformation gradient is then given as:

$$\boldsymbol{F} = \boldsymbol{\nabla\chi} \tag{1}$$

where $\boldsymbol{\nabla}$ denotes gradient with respect to the material point, $\mathbf{X}$ in the undeformed body. $\boldsymbol{F}$ can be decomposed into elastic and plastic parts, $\boldsymbol{F^e}$ **and** $\boldsymbol{F^p}$ respectively (commonly referred to as Kroner decomposition):

$$\boldsymbol{F} = \boldsymbol{F^e F^p} \tag{2}$$

We assume that elastic deformation can only lead to an increase in volume, i.e.

$$J^e \equiv det(\boldsymbol{F^e}) > 0 \tag{3}$$

We also assume that the plastic deformation is incompressible, i.e.

$$J^p \equiv det(\boldsymbol{F^p}) = 1 \tag{4}$$

The right Polar decomposition of $\boldsymbol{F^e}$ is given as:

$$\boldsymbol{F^e} = \boldsymbol{R^e U^e} \tag{5}$$

where $\boldsymbol{R^e}$ is the rotation tensor and $\boldsymbol{U^e}$ is a symmetric positive-definite tensor, called the elastic right stretch tensor. The spatial velocity gradient, $\boldsymbol{L}$ defined as:

$$\boldsymbol{L} \equiv \boldsymbol{grad\, v} = \dot{\boldsymbol{F}}\boldsymbol{F^{-1}} \tag{6}$$

where $\boldsymbol{grad}$ represents the gradient in with respect to the spatial point, $\boldsymbol{x}$ in the deformed body. Substituting the Kroner decomposition of deformation gradient from (2) into (6), the velocity gradient can be decomposed as:

$$\boldsymbol{L} = \dot{\boldsymbol{F}}^{\boldsymbol{e}}\boldsymbol{F^{e-1}} + \boldsymbol{F^e}\dot{\boldsymbol{F}}^{\boldsymbol{p}}\boldsymbol{F^{p-1}F^{e-1}} = \boldsymbol{L^e} + \boldsymbol{F^e L^p F^{e-1}} \tag{7}$$

with $\boldsymbol{L^e} = \dot{\boldsymbol{F}}^{\boldsymbol{e}}\boldsymbol{F^{e-1}}$ and $\boldsymbol{L^p} = \dot{\boldsymbol{F}}^{\boldsymbol{p}}\boldsymbol{F^{p-1}}$. We define the stretching ($\boldsymbol{D}$) and spin ($\boldsymbol{W}$) tensors as:

$$\begin{aligned} \boldsymbol{D^e} &\equiv sym(\boldsymbol{L^e}) \\ \boldsymbol{W^e} &\equiv skw(\boldsymbol{L^e}) \\ \boldsymbol{D^p} &\equiv sym(\boldsymbol{L^p}) \\ \boldsymbol{W^p} &\equiv skw(\boldsymbol{L^p}) \end{aligned} \tag{8}$$

We assume that the plastic flow is irrotational, i.e.

$$\boldsymbol{W^p} = \boldsymbol{0} \tag{9}$$

so that $\boldsymbol{L^p} = \boldsymbol{D^p}$.

First Law of Thermodynamics

The First Law of Thermodynamics states that the change in internal energy of an isolated system is equal to the work done on the system plus the heat added to the system. In the reference configuration, the local form of first law is written as:

$$\dot{e_R} = \boldsymbol{T_0}\colon \dot{\boldsymbol{F}} - Div\,(\boldsymbol{q_R}) + r_R \tag{10}$$

where subscript 'R' indicates reference configuration. e_R is the internal energy per unit, $\boldsymbol{q_R}$ is the heat flux vector and r_R is the heat supply per unit volume. $\boldsymbol{T_0}$ is the unsymmetric 1st Piola-Kirchhoff stress tensor and $\boldsymbol{T_0}\colon \dot{\boldsymbol{F}}$ is the stress power. Stress power can also be written in terms of Cauchy stress as:

$$\boldsymbol{T}_0\colon \dot{\boldsymbol{F}} = J\boldsymbol{T}\boldsymbol{F}^{-\boldsymbol{T}}\colon \dot{\boldsymbol{F}} = J^e\boldsymbol{T}\colon \dot{\boldsymbol{F}}\boldsymbol{F}^{-\boldsymbol{1}} = J^e\boldsymbol{T}\colon \boldsymbol{L} \tag{11}$$

Hence, the first law can be re-written as:

$$\dot{e_R} = J\boldsymbol{T}\colon \boldsymbol{L} - Div\,(\boldsymbol{q_R}) + r_R \tag{12}$$

Second Law of Thermodynamics

The Second Law of Thermodynamics states that the net entropy production of an isolated system is non-negative. Therefore, the local form of second law in the reference configuration is written as:

$$\delta_{\mathrm{R}} = \dot{\eta}_R + Div\left(\frac{\boldsymbol{q_R}}{\theta}\right) - \frac{r_R}{\theta} \geq 0 \tag{13}$$

where η_R is entropy per unit volume, δ_R is entropy production per unit volume, and θ is the temperature. The first term on the right is the rate of change of internal entropy of the system and the second and third terms on the right add up to the entropy flow into the system.

Free-energy Imbalance

We know that the Helmholtz free energy is related to the internal energy and entropy through the following relation:

$$\psi_R = e_R - \eta_R\theta \tag{14}$$

ψ_R is the Helmholtz energy per unit volume. Hence, the change in free energy is given as:

$$\dot{\psi_R} = \dot{e_R} - \dot{\eta_R}\theta - \eta_R\dot{\theta} \tag{15}$$

Substitute $\dot{e_R}$ from equation (12) and $\dot{\eta_R}$ from equation (13) into equation (15):

$$\dot{\psi_R} + \eta_R\dot{\theta} - J\boldsymbol{T}\colon \boldsymbol{L} + \frac{1}{\theta}\boldsymbol{q}.\boldsymbol{\nabla T} = -\theta\delta_R \leq 0 \tag{16}$$

Equation (16) is called the local free-energy imbalance inequality. $\theta\delta_R$ represents dissipation per unit volume and the free-energy imbalance states that dissipation is non-negative.

We derive two new stress measures from the Cauchy stress tensor, **T**. Consider the stress power term $J\boldsymbol{T}:\boldsymbol{L}$. Using equation (7), the stress power can be decomposed into elastic and plastic terms:

$$J\boldsymbol{T}:\boldsymbol{L} = J\boldsymbol{T}:\boldsymbol{L^e} + J\boldsymbol{T}:\boldsymbol{F^e L^p F^{e-1}} = J\boldsymbol{T}:\boldsymbol{D^e} + J\boldsymbol{F^{e^T} T F^{e-T}}:\boldsymbol{L^p} \tag{17}$$

Since the strains are defined in the reference configuration in terms of **U**, we would like to find $\boldsymbol{D^e}$ in terms of $\dot{\boldsymbol{U}}^{\boldsymbol{e}}$ or $\dot{\boldsymbol{C}}^{\boldsymbol{e}}$. Consider the time derivative of the Right Cauchy Green tensor, $\dot{\boldsymbol{C}}^{\boldsymbol{e}}$:

$$\begin{aligned}\dot{\boldsymbol{C}}^{\boldsymbol{e}} &= \overline{\dot{\boldsymbol{F}}^{\boldsymbol{e^T}}\boldsymbol{F^e}} \\ &= \boldsymbol{F^{e^T}}\left(\boldsymbol{L^e} + \boldsymbol{L^{e^T}}\right)\boldsymbol{F^e} \\ &= 2\boldsymbol{F^{e^T} D^e F^e}\end{aligned} \tag{18}$$

$$\boldsymbol{D^e} = \frac{1}{2}\boldsymbol{F^{e-T}}\dot{\boldsymbol{C}}^{\boldsymbol{e}}\boldsymbol{F^{e-1}} \tag{19}$$

Substituting $\boldsymbol{D^e}$ from (19) into (17), we have:

$$J\boldsymbol{T}:\boldsymbol{L} = \left(J\boldsymbol{F^{e-1} T F^{e-T}}\right):\frac{\dot{\boldsymbol{C}}^{\boldsymbol{e}}}{2} + \left(J\boldsymbol{F^{e^T} T F^{e-T}}\right):\boldsymbol{L^p} \tag{20}$$

At this juncture, we define two new stress measures:

$$\boldsymbol{T^e} = J\boldsymbol{F^{e-1} T F^{e-T}} \tag{21}$$

$$\boldsymbol{M^e} = J\boldsymbol{F^{e^T} T F^{e-T}} = \boldsymbol{C^e T^e} \tag{22}$$

where $\boldsymbol{T^e}$ is the symmetric elastic 2nd Piola-Kirchhoff stress, and $\boldsymbol{M^e}$ is the Mandel stress. Hence, the stress power can be re-written as:

$$J\boldsymbol{T}:\boldsymbol{L} = \boldsymbol{T^e}:\frac{\dot{\boldsymbol{C}}^{\boldsymbol{e}}}{2} + \boldsymbol{M^e}:\boldsymbol{L^p} \tag{23}$$

Re-writing the first law from equation (12) in terms of the two new stress measures introduced above:

$$\dot{e_R} = \boldsymbol{T^e}:\frac{\dot{\boldsymbol{C}}^{\boldsymbol{e}}}{2} + \boldsymbol{M^e}:\boldsymbol{L^p} - Div\,(\boldsymbol{q_R}) + r_R \tag{24}$$

The constitutive laws for e_R, ψ_R, $\boldsymbol{T^e}$, $\boldsymbol{M^e}$ are assumed to be functions of the same set of variables $(\boldsymbol{C^e}, \theta, \boldsymbol{\nabla}\theta, \boldsymbol{\xi})$ where $\boldsymbol{\xi}$ represents the internal hardening variable tensor.

$$\begin{aligned} e_R &= \hat{e}_R(\boldsymbol{C^e}, \theta, \boldsymbol{\nabla}\theta, \boldsymbol{\xi}) \\ \psi_R &= \hat{\psi}_R(\boldsymbol{C^e}, \theta, \boldsymbol{\nabla}\theta, \boldsymbol{\xi}) \\ \eta_R &= \hat{\eta}_R(\boldsymbol{C^e}, \theta, \boldsymbol{\nabla}\theta, \boldsymbol{\xi}) \\ \boldsymbol{T^e} &= \widehat{\boldsymbol{T^e}}(\boldsymbol{C^e}, \theta, \boldsymbol{\nabla}\theta, \boldsymbol{\xi}) \\ \boldsymbol{M^e} &= \widehat{\boldsymbol{M^e}}(\boldsymbol{C^e}, \theta, \boldsymbol{\nabla}\theta, \boldsymbol{\xi}) \end{aligned} \tag{25}$$

Taking the time derivative of free energy,

$$\dot{\psi_R} = \frac{\partial\hat{\psi}_R}{\partial\boldsymbol{C^e}}:\dot{\boldsymbol{C}}^{\boldsymbol{e}} + \frac{\partial\hat{\psi}_R}{\partial\theta}\dot{\theta} + \frac{\partial\hat{\psi}_R}{\partial\boldsymbol{\nabla}\theta}.\dot{\overline{\boldsymbol{\nabla}\theta}} + \frac{\partial\hat{\psi}_R}{\partial\boldsymbol{\xi}} * \dot{\boldsymbol{\xi}} \tag{26}$$

where '$*$' denotes the appropriate scalar product considering the order of the internal variable tensor, $\boldsymbol{\xi}$. Using equation (16), the rate of change of free energy can also be written as:

$$\dot{\psi_R} = \boldsymbol{T^e}:\frac{\dot{\boldsymbol{C}}^{\boldsymbol{e}}}{2} + \boldsymbol{M^e}:\boldsymbol{L^p} - \eta_R\dot{\theta} - \frac{1}{\theta}\boldsymbol{q}.\boldsymbol{\nabla}\theta - \theta\delta_R \tag{27}$$

Combining equations (26) and (27),

$$\left(\frac{\partial\hat{\psi}_R}{\partial \boldsymbol{C}^e} - \boldsymbol{T}^e\right) : \dot{\boldsymbol{C}}^e + \left(\frac{\partial\hat{\psi}_R}{\partial\theta} + \eta_R\right)\dot{\theta} + \frac{\partial\hat{\psi}_R}{\partial \boldsymbol{\nabla}\theta} . \overline{\dot{\boldsymbol{\nabla}\theta}} + \left(\frac{\partial\hat{\psi}_R}{\partial \boldsymbol{\xi}} * \dot{\boldsymbol{\xi}} + \frac{1}{\theta}\boldsymbol{q} . \boldsymbol{\nabla}\theta - \boldsymbol{M}^e : \boldsymbol{L}^p + \theta\delta_{\mathrm{R}}\right) = 0 \tag{28}$$

Using the Coleman-Noll procedure, one can deduce the following definitions for stress and entropy:

$$\boldsymbol{T}^e = 2\frac{\partial\hat{\psi}_R}{\partial \boldsymbol{C}^e} \tag{29}$$

$$\eta_R = -\frac{\partial\hat{\psi}_R}{\partial\theta} \tag{30}$$

$$\frac{\partial\hat{\psi}_R}{\partial \boldsymbol{\nabla}\theta} = \boldsymbol{0} \tag{31}$$

In view of the above relations, the second law reduces to:

$$\frac{\partial\hat{\psi}_R}{\partial \boldsymbol{\xi}} * \dot{\boldsymbol{\xi}} + \frac{1}{\theta}\boldsymbol{q} . \boldsymbol{\nabla}\theta - \boldsymbol{M}^e : \boldsymbol{L}^p = -\theta\delta_{\mathrm{R}} \leq 0 \tag{32}$$

Temperature Evolution Equation

Now, we work towards finding an evolution equation for temperature. Consider the time derivative of internal energy and use the thermodynamic relations derived in equations (29) and (30).

$$\begin{aligned}
\dot{e}_R &= \dot{\psi}_R + \theta\dot{\eta}_R + \dot{\theta}\eta_R \\
\dot{e}_R &= \frac{\partial\hat{\psi}_R}{\partial \boldsymbol{C}^e} : \dot{\boldsymbol{C}}^e + \frac{\partial\hat{\psi}_R}{\partial\theta}\dot{\theta} + \frac{\partial\hat{\psi}_R}{\partial \boldsymbol{\xi}} * \dot{\boldsymbol{\xi}} - \theta\overline{\frac{\partial\dot{\hat{\psi}}_R}{\partial\theta}} + \dot{\theta}\eta_R \\
\dot{e}_R &= \frac{\boldsymbol{T}^e}{2} : \dot{\boldsymbol{C}}^e + \frac{\partial\hat{\psi}_R}{\partial \boldsymbol{\xi}} * \dot{\boldsymbol{\xi}} - \frac{\theta}{2}\frac{\partial \boldsymbol{T}^e}{\partial\theta} : \dot{\boldsymbol{C}}^e - \theta\frac{\partial^2\hat{\psi}_R}{\partial\theta^2}\dot{\theta} - \theta\frac{\partial^2\hat{\psi}_R}{\partial \boldsymbol{\xi}\partial\theta} * \dot{\boldsymbol{\xi}} \\
\dot{e}_R &= \frac{\boldsymbol{T}^e}{2} : \dot{\boldsymbol{C}}^e - \frac{\theta}{2}\frac{\partial \boldsymbol{T}^e}{\partial\theta} : \dot{\boldsymbol{C}}^e + \left(\frac{\partial\hat{\psi}_R}{\partial \boldsymbol{\xi}} - \theta\frac{\partial^2\hat{\psi}_R}{\partial \boldsymbol{\xi}\partial\theta}\right) * \dot{\boldsymbol{\xi}} - \theta\frac{\partial^2\hat{\psi}_R}{\partial\theta^2}\dot{\theta}
\end{aligned} \tag{33}$$

Substituting $\dot{e}_R$ from the first law (equation (24)) and rearranging terms,

$$-Div\,(\boldsymbol{q_R}) + r_R + \underbrace{\left(\frac{\theta}{2}\frac{\partial \boldsymbol{T}^e}{\partial\theta} : \dot{\boldsymbol{C}}^e\right)}_{\dot{q}^e} + \underbrace{\left[\boldsymbol{M}^e : \boldsymbol{L}^p - \left(\frac{\partial\hat{\psi}_R}{\partial \boldsymbol{\xi}} - \theta\frac{\partial^2\hat{\psi}_R}{\partial \boldsymbol{\xi}\partial\theta}\right) * \dot{\boldsymbol{\xi}}\right]}_{\dot{q}^p} = \underbrace{-\theta\frac{\partial^2\hat{\psi}_R}{\partial\theta^2}\dot{\theta}}_{c_R\dot{\theta}} \tag{34}$$

$$-Div\,(\boldsymbol{q_R}) + r_R + \dot{q}^e + \dot{q}^p = c_R\dot{\theta} \tag{35}$$

where $\dot{q}^e$ is rate of heating due to thermo-elasticity, $\dot{q}^p$ represents rate of inelastic heating and c_R is the specific heat capacity, defined at constant strain and constant internal variables. More specifically, c_R is specific heat capacity times reference density. Equation (34) is the evolution equation for temperature. The first term in the expression for $\dot{q}^p$, i.e. $\boldsymbol{M}^e : \boldsymbol{L}^p$ represents rate of plastic work while the remainder of $\dot{q}^p$ represents the rate of change of internal energy of cold work ($\left(\frac{\partial\hat{\psi}_R}{\partial \boldsymbol{\xi}} - \theta\frac{\partial^2\hat{\psi}_R}{\partial \boldsymbol{\xi}\partial\theta}\right) * \dot{\boldsymbol{\xi}}$). We define a parameter, β, that quantifies the amount of plastic work converted to heat, i.e.

$$\beta = \frac{\dot{q_p}}{\boldsymbol{M^e}:\boldsymbol{L^p}} \tag{36}$$

β is often called the Taylor-Quinney coefficient. β is dependent on the evolution of internal variables and hence is dependent on the history of loading. However, in most applications, it is assumed to be a constant. A new measure of thermomechanical coupling, called the Gruneisen tensor, is defined:

$$\boldsymbol{\Gamma}_{\mathrm{R}} = -\frac{1}{c_R}\left(\frac{\partial \boldsymbol{T^e}}{\partial \theta}\right)_{\boldsymbol{C^e},\boldsymbol{\xi}} \tag{37}$$

Fourier's Law of heat conduction gives the following relation between heat flux and temperature gradient:

$$\mathbf{q_R} = -k\boldsymbol{\nabla}\theta \tag{38}$$

where k is the thermal conductivity. Ideally, the thermal conductivity is a tensor dependent on temperature. However, we assume thermal isotropy and no dependence of thermal conductivity on temperature, which may not be a bad assumption for moderate temperature changes.

Substituting relations from (36), (37) and (38) into (34) and ignoring the heat supply term (i.e.
$r_R = 0$),

$$k\nabla^2\theta - \frac{c_R\theta}{2}\boldsymbol{\Gamma}_{\mathrm{R}}:\dot{\boldsymbol{C}}^{\boldsymbol{e}} + \beta\boldsymbol{M^e}:\boldsymbol{L^p} = c\dot{\theta} \tag{39}$$

Assuming plastic irrotationality (equation (9)), we have $\boldsymbol{L^p} = \boldsymbol{D^p}$. Using a co-directional flow rule, the plastic stretch-rate, $\boldsymbol{D^p}$ can be written as:

$$\boldsymbol{D^p} = \frac{3}{2}\,\dot{\bar{\epsilon}}^p\,\frac{\boldsymbol{M_0^e}}{\bar{\sigma}} \tag{40}$$

where $\boldsymbol{M_0^e}$ is the deviatoric portion of Mandel stress, $\dot{\bar{\epsilon}}^p$ is the effective plastic strain rate and $\bar{\sigma}$ is the effective stress, defined below:

$$\dot{\bar{\epsilon}}^p = \sqrt{\frac{2}{3}}|\boldsymbol{D^p}| \tag{41}$$

$$\bar{\sigma} = \sqrt{\frac{3}{2}}\,|\boldsymbol{M_0^e}| \tag{42}$$

Hence, the rate of plastic work can be simplified as:

$$\boldsymbol{M^e}:\boldsymbol{L^p} = \boldsymbol{M^e}:\boldsymbol{D^p} = \bar{\sigma}\dot{\bar{\epsilon}}^p \tag{43}$$

The temperature evolution can then be put into most simplified form below:

$$k\nabla^2\theta - \frac{c\theta}{2}\boldsymbol{\Gamma}:\dot{\boldsymbol{C}}^{\boldsymbol{e}} + \beta\bar{\sigma}\dot{\bar{\epsilon}}^p = c_R\dot{\theta} \tag{44}$$

CONSTITUTIVE MODELING

We define our constitutive model in terms of a logarithmic strain in the undeformed configuration. It is defined below, in terms of the right stretch tensor, $\boldsymbol{U^e}$.

$$\boldsymbol{E^e} \equiv \ln(\boldsymbol{U^e}) \tag{45}$$

Logarithmic strains are used because they facilitate an additive decoupling of volumetric and deviatoric strains under large pressures which is not possible with Green-Lagrange Strains.

Furthermore, with the use of a correct invariant basis, the stress terms can also be decomposed into pressure and deviatoric response terms, as shown below. This is extremely helpful in a direct incorporation of a complete equation of state, which is typically measured through a separate set of experiments.

Assuming that the material is isotropic, the constitutive response of sucrose is defined though an elastic free energy per unit volume, ψ_R. In general, ψ_R is a function of the elastic Right Cauchy-Green tensor, $\boldsymbol{C^e}$ and temperature, θ but for an isotropic material, the free energy can be represented in terms of 3 principal stretches ($\psi_R = \tilde{\psi}_R(\lambda_1^e, \lambda_2^e, \lambda_3^e, \theta)$) or 3 principal invariants of $\boldsymbol{C^e}$, ($\psi_R = \tilde{\psi}_R(I_1, I_2, I_3, \theta)$) where $I_1 = tr\boldsymbol{C^e}$, $I_2 = 0.5 \times \left[(tr\boldsymbol{C^e})^2 + tr\boldsymbol{C^{e2}}\right]$ and $I_3 = \det \boldsymbol{C^e} = J^{e2}$. With the (I_1, I_2, I_3) principal invariant based free energy, it is not possible to isolate the effect of each invariant due to the non-orthogonality of different stress response terms. Therefore, the free energy density is written in terms of a new set of logarithmic strain invariants (K_1, K_2, K_3), as proposed by (Criscione et al. 2000). With each of these invariants, one can associate specific aspects of deformation and isolate the effect of each. The first invariant, K_1, defined below represents the volume change.

$$K_1 = tr(\boldsymbol{E^e}) = \ln(J^e) \tag{46}$$

where the superscript 'e' represents elastic. The second invariant, K_2 represents the distortional response of the material under constant volume and is defined as the magnitude of deviatoric portion of logarithmic strain.

$$K_2 = |\boldsymbol{E_0^e}| \tag{47}$$

Since, $\boldsymbol{E^e} = \frac{K_1}{3}\boldsymbol{I} + \boldsymbol{E_0^e}$, a tensorial direction can be associated with this deviatoric strain invariant:

$$\boldsymbol{N} = \frac{\boldsymbol{E_0^e}}{|\boldsymbol{E_0^e}|} \tag{48}$$

where $\boldsymbol{N}$ is a unit tensor. Hence, the strain can be written as $\boldsymbol{E^e} = \frac{K_1}{3}\boldsymbol{I} + K_2\boldsymbol{N}$. The third invariant, K_3 represents the mode of distortion and is defined below:

$$K_3 = 3\sqrt{6}\det(\boldsymbol{N}) \tag{49}$$

It can be noted that $K_1 > 0$ for dilatation and $K_1 < 0$ under compression. $K_2 \geq 0$ always holds whereas $-1 \leq K_3 \leq 1$. $K_3 = 1$ in simple tension, $K_3 = -1$ in simple compression and $K_3 = 0$ in simple shear.

Let $\tilde{\psi}_R(K_1, K_2, K_3, \theta)$ be the free energy density. It can be shown that Mandel stress and logarithmic strain in reference configuration are power conjugates. Hence,

$$\boldsymbol{M^e} = \frac{\partial \tilde{\psi}_R}{\partial \boldsymbol{E^e}} = \left(\frac{\partial \tilde{\psi}_R}{\partial K_1}\boldsymbol{I} + \frac{\partial \tilde{\psi}_R}{\partial K_2}\boldsymbol{N} + \frac{\partial \tilde{\psi}_R}{\partial K_3}\boldsymbol{Y}\right) \tag{50}$$

$$\boldsymbol{Y} = 3\sqrt{6}\boldsymbol{N^2} - \sqrt{6}\boldsymbol{I} - 3K_3\boldsymbol{N} \tag{51}$$

Since the tensors, $\boldsymbol{C^e}$ and $\boldsymbol{T^e}$ coaxial, i.e. have the same principal directions, Cauchy stress can be found using the definition of Mandel stress in equation (22),

$$\boldsymbol{T} = \frac{1}{J}\boldsymbol{R^e M^e R^{eT}} = \frac{1}{J}\left(\frac{\partial \tilde{\psi}_R}{\partial K_1}\boldsymbol{I} + \frac{\partial \tilde{\psi}_R}{\partial K_2}\boldsymbol{n} + \frac{\partial \tilde{\psi}_R}{\partial K_3}\boldsymbol{y}\right) \tag{52}$$

Where $\boldsymbol{n} = \boldsymbol{R^e N R^{eT}}$ and $\boldsymbol{y} = \boldsymbol{R^e Y R^{eT}}$. Note that $\boldsymbol{n}:\boldsymbol{I} = \boldsymbol{0}, \boldsymbol{y}:\boldsymbol{I} = \boldsymbol{0}$ and $\boldsymbol{n}:\boldsymbol{y} = \boldsymbol{0}$, i.e. the Cauchy stress is composed of three mutually orthogonal terms and each term is dependent on

derivative of a different stress invariant. This is facilitated by using a logarithmic strain measure and an appropriate set of invariants for logarithmic strain. So, it is possible to easily isolate the three response terms by contracting with $\boldsymbol{I}, \boldsymbol{n}$ and $\boldsymbol{y}$. Specifically, the first term in (52) corresponds to the pressure term while the other two terms add up to give the deviatoric stress.

$$\frac{\boldsymbol{T}:\boldsymbol{I}}{3} = -P = \frac{1}{J}\frac{\partial \tilde{\psi}_R}{\partial K_1} \tag{53}$$

So, the pressure term can be isolated from the deviatoric response easily, while retaining the its dependence on all three invariants and temperature, i.e. $P(K_1, K_2, K_3, \theta)$.

The free energy density, $\tilde{\psi}_R(K_1, K_2, K_3, \theta)$ can be additively decomposed into three parts: (a) purely volumetric, $f_1(K_1, \theta)$, (b) purely distortional, $f_2(K_2, K_3, \theta)$ and (c) coupled-volumetric/distortional, $f_3(K_1, \theta) f_4(K_2, K_3, \theta)$, where the temperature dependence is retained in each portion of the free energy density.

$$\tilde{\psi}_R(K_1, K_2, K_3, \theta) = f_1(K_1, \theta) + f_2(K_2, K_3, \theta) + f_3(K_1, \theta) f_4(K_2, K_3, \theta) \tag{54}$$

For the purpose of modeling sucrose, we consider a very simple form of free energy of the following form:

$$\tilde{\psi}_R(K_1, K_2, K_3, \theta) = f_1(K_1, \theta) + G(K_1, \theta) K_2^2 \tag{55}$$

where $G(K_1, \theta)$ is the temperature and volumetric strain-dependent shear modulus. The first term in the free-energy expression leads to pressure through $P(K_1, \theta) = -\frac{1}{J}\frac{\partial f_1}{\partial K_1} - \frac{1}{J}\frac{\partial G}{\partial K_1} K_2^2$. Pressure is found through a complete equation of state as described in section 4. Generally, the contribution of shear-induced pressure ($-\frac{1}{J}\frac{\partial G}{\partial K_1} K_2^2$) is very small due to small pressure dependent coefficient of shear modulus and small elastic distortional strains and can therefore be ignored. Therefore, the Mandel stress and Cauchy stress for such a free energy density function can be calculated as:

$$\boldsymbol{M^e} = -P(K_1, \theta) J \boldsymbol{I} + 2G(K_1, \theta) K_2 \boldsymbol{N} \tag{56}$$

$$\boldsymbol{T}(K_1, K_2, \theta) = -P(K_1, \theta)\boldsymbol{I} + \frac{2}{J} G(K_1, \theta) K_2 \boldsymbol{n} \tag{57}$$

Since $\boldsymbol{L^p} = \boldsymbol{D^p}$ and $\boldsymbol{L^p} = \dot{\boldsymbol{F}}^{\boldsymbol{p}} \boldsymbol{F}^{\boldsymbol{p}^{-1}}$, the evolution of plastic distortion, $\boldsymbol{F^p}$ is given through the following equation:

$$\dot{\boldsymbol{F}}^{\boldsymbol{p}} = \boldsymbol{D^p F^p} \tag{58}$$

The plastic stretching, $\boldsymbol{D^p}$ is then given through a codirectional flow rule, $\boldsymbol{D^p} = \frac{3}{2}\, \dot{\bar{\epsilon}}^p \frac{\boldsymbol{M_0^e}}{\bar{\sigma}}$ (equation (40)). The effective plastic strain-rate and the equivalent stress are related through a strain-rate and temperature-dependent constitutive law. We use a Johnson-Cook model here:

$$\bar{\sigma} = [A + B(\bar{\epsilon}^p)^n]\left[1 + C \ln\left(\frac{\dot{\bar{\epsilon}}^p}{\dot{\bar{\epsilon}}_0}\right)\right](1 - \hat{\theta}^m) \tag{59}$$

where $(A, B, n, C, \dot{\bar{\epsilon}}_0, m)$ are material parameters, $\hat{\theta}$ is a function of temperature, θ and pressure, P defined below:

$$\hat{\theta} = \frac{\theta - \theta_{ref}}{\theta_m(P) - \theta_{ref}} \tag{60}$$

θ_{ref} is the reference temperature (usually taken to be the room temperature) and θ_m is the melt temperature. Since high pressures are achieved in the experiments and temperatures are expected to go beyond melting, the dependence of melting temperature on pressure is taken into account.

Moreover, the melting point of large organic molecules like HMX and sucrose is highly dependent on pressure. Melting point is typically described by Lindemann Law.

$$\theta_m = \theta_{m0} \exp\left[2\Gamma_0(1-J) + \frac{2}{3} ln(J)\right] \tag{61}$$

where θ_{m0} is melting temperature at ambient pressure, Γ_0 is the Gruneisen parameter at ambient pressure and temperature, and $J = \frac{v}{v_0}$ is the compression ratio. v is the final specific volume and v_0 is the initial specific volume. A linearized version of the Lindemann Law, called the Kraut-Kennedy relation is used here:

$$\theta_m = \theta_{m0} \left(1 + a\frac{\Delta v}{v_0}\right) \tag{62}$$

where Δv is the reduction in specific volume under compression and a is a constant defined as:

$$a = 2\left(\Gamma_0 - \frac{1}{3}\right) \tag{63}$$

COMPLETE MIE-GRUNEISEN EQUATION OF STATE

The Mie-Gruneisen equation of state has been one of the most commonly used forms of an equation of state for a solid subjected to shock loading. It is often encountered in hydrocodes, for solids under pressures up to a few megabar. In this section, we present a derivation of a complete equation of state, i.e. with a temperature dependent specific heat capacity, on lines with the work by (Menikoff 2016). Note: The equation of state is derived in the spatial/deformed configuration as opposed to the reference/undeformed configuration used in Section 2 and Section 3. In deriving the equation of state, we assume a state of purely volumetric deformation.

The Gruneisen model can be derived from the definition of the Gruneisen parameter, Γ:

$$\Gamma \equiv v\left(\frac{\partial P}{\partial e}\right)_v \tag{64}$$

where the Gruneisen scalar parameter defined above is the volumetric part of the spatial Gruneisen tensor defined below:

$$\boldsymbol{\Gamma} = -\frac{v}{c}\left(\frac{\partial \boldsymbol{T}}{\partial \theta}\right)_{\boldsymbol{c}^e,\boldsymbol{\xi}} \tag{65}$$

$\boldsymbol{T}$ is Cauchy stress and c is the specific heat capacity. If the Gruneisen parameter is assumed to be independent of pressure and specific internal energy, equation (64) can be integrated to obtain the usually encountered form of Mie-Gruneisen equation of state.

$$P - P_{ref} = \frac{\Gamma}{v}(e - e_{ref}) \tag{66}$$

where P_{ref} and e_{ref} lie on a reference curve.

In order to specify a complete equation of state, we consider the thermodynamic variables like η, e, ψ and P as functions of v and θ, i.e.

$$\begin{aligned} \eta &= \eta(v,\theta) \\ e &= e(v,\theta) \\ \psi &= \psi(v,\theta) \\ P &= P(v,\theta) \end{aligned} \tag{67}$$

Suppose we start with an initial state characterized by the set of thermodynamic variables $(v_0, \theta_0, \eta_0, e_0, \psi_0, P_0)$. Let the final thermodynamic state be represented by $(v, \theta, \eta, e, \psi, P)$. Since a complete equation of state should be independent of the thermodynamic path connecting the initial and final states, we choose a path shown in 9. The path consists of 2 segments: an isotherm at $\theta = \theta_0$ followed by an isochore at $v = v$.

Differential change in entropy can be written as:

$$d\eta = \left(\frac{\partial \eta}{\partial v}\right)_\theta dv + \left(\frac{\partial \eta}{\partial \theta}\right)_v d\theta \tag{68}$$

where subscripts denote that the independent variables are held constant when partial derivatives are taken. The partial derivatives of entropy can be written in terms of known/measurable thermodynamic quantities, Γ and c_v. The specific heat capacity, c_v is defined as:

$$c_v = \left(\frac{\partial e}{\partial \theta}\right)_v \tag{69}$$

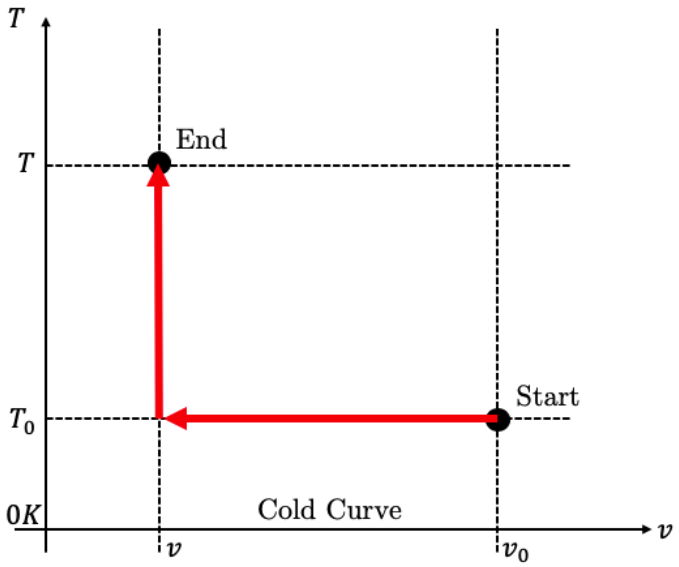

Figure 9 A thermodynamic path connecting the initial and final states.

From the first law of thermodynamics, we have,

$$de = -Pdv + \theta d\eta \tag{70}$$

If (v, η) are taken as independent variables, then the differential of specific internal energy, $e = e(v, \eta)$, can be written as:

$$de = \left(\frac{\partial e}{\partial v}\right)_\eta dv + \left(\frac{\partial e}{\partial \eta}\right)_v d\eta \tag{71}$$

Since dv and $d\eta$ are arbitrary, we can define pressure and temperature in terms of partial derivatives of specific internal energy, from equations (70) and (71).

$$P = -\left(\frac{\partial e}{\partial v}\right)_\eta \tag{72}$$

$$\theta = \left(\frac{\partial e}{\partial \eta}\right)_v \tag{73}$$

If (v,θ) are instead chosen as free variables, the differential of specific internal energy and specific entropy can be written as:

$$de = \left(\frac{\partial e}{\partial v}\right)_\theta dv + \left(\frac{\partial e}{\partial \theta}\right)_v d\theta = \left(\frac{\partial e}{\partial v}\right)_\theta dv + c_v d\theta \tag{74}$$

$$d\eta = \left(\frac{\partial \eta}{\partial v}\right)_\theta dv + \left(\frac{\partial \eta}{\partial \theta}\right)_v d\theta \tag{75}$$

Substituting $d\eta$ from (75) into (71),

$$de = \left[-P + \theta\left(\frac{\partial \eta}{\partial v}\right)_\theta\right] dv + \left[\theta\left(\frac{\partial \eta}{\partial \theta}\right)_v\right] d\theta \tag{76}$$

Comparing (74) and (76),

$$\left(\frac{\partial e}{\partial v}\right)_\theta = \left[-P + \theta\left(\frac{\partial \eta}{\partial v}\right)_\theta\right] \tag{77}$$

$$c_v = \theta\left(\frac{\partial \eta}{\partial \theta}\right)_v \tag{78}$$

Using Maxwell's relations, we have

$$\left(\frac{\partial \eta}{\partial v}\right)_\theta = \left(\frac{\partial P}{\partial \theta}\right)_v \tag{79}$$

From equations (64), (78) and (79), one can show that

$$\Gamma c_v = v\left(\frac{\partial P}{\partial \theta}\right)_v = v\left(\frac{\partial \eta}{\partial v}\right)_\theta \tag{80}$$

Substituting the above relation into (77), it can be shown that

$$\left(\frac{\partial e}{\partial v}\right)_\theta = \left[-P + \frac{\Gamma c_v \theta}{v}\right] \tag{81}$$

Now we aim to find a differential change in entropy from equation (75) in terms of measurable quantities. Substituting expressions for partial derivatives from equations (78) and (80) into (75):

$$d\eta = \frac{\Gamma c_v}{v} dv + \frac{c_v}{\theta} d\theta \tag{82}$$

Integrating the above equation along the thermodynamic path in Figure 1, entropy at the final state can be written as:

$$\eta(v,\theta) = \eta_0 + \int_{v_0}^{v} \frac{\Gamma(v',\theta_0) c_v(v',\theta_0)}{v'} dv' + \int_{\theta_0}^{\theta} \frac{c_v(v,\theta')}{\theta'} d\theta' \tag{83}$$

where the Gruneisen parameter, Γ and specific heat capacity, c_v are considered as functions of (v,θ). Similarly, consider specific Helmholtz free energy, $\psi(v,\theta)$. Differential change in free energy is given as:

$$d\psi = -P dv - \eta d\theta \tag{84}$$

where

$$P = -\left(\frac{\partial \psi}{\partial v}\right)_\theta \tag{85}$$

$$\eta = -\left(\frac{\partial \psi}{\partial \theta}\right)_v \tag{86}$$

Integrate (84) and substitute the expression for entropy, $\eta(v,\theta)$ from (86).

$$\psi(v,\theta) = \psi_0 - \int_{v_0}^{v} P(v',\theta_0)dv' - \int_{\theta_0}^{\theta}\left[\eta_0 + \int_{v_0}^{v}\frac{\Gamma(\mathrm{v}',\theta_0)c_v(v',\theta_0)}{v'}dv' + \int_{\theta_0}^{\theta'}\frac{c_v(v,\theta'')}{\theta''}d\theta''\right]d\theta' \tag{87}$$

Integrating the last term in (87) by parts, one can obtain a general expression for specific free energy:

$$\psi(v,\theta) = \psi_0 - \eta_0(\theta-\theta_0) - \int_{v_0}^{v}\left[P(v',\theta_0) + (\theta-\theta_0)\frac{\Gamma(\mathrm{v}',\theta_0)c_v(v',\theta_0)}{v'}\right]dv' - \int_{\theta_0}^{\theta}\frac{(\theta-\theta')}{\theta'}c_v(v,\theta')d\theta' \tag{88}$$

Pressure can be obtained from specific free energy, using equation (85):

$$P(v,\theta) = -\left(\frac{\partial\psi}{\partial v}\right)_\theta = P(v,\theta_0) + (\theta-\theta_0)\frac{\Gamma(v,\theta_0)c_v(v,\theta_0)}{v} + \int_{\theta_0}^{\theta}\frac{(\theta-\theta')}{\theta'}\frac{\partial c_v(v,\theta')}{\partial v}d\theta' \tag{89}$$

Compatibility condition: The Gruneisen coefficient and specific heat are not fully independent. They must obey the thermodynamic compatibility equation derived below.

$$\frac{\partial}{\partial v}\left(\frac{\partial^2\psi}{\partial\theta^2}\right) = \frac{\partial}{\partial\theta}\left(\frac{\partial^2\psi}{\partial\theta\partial v}\right) \tag{90}$$

To move further, we need to prove a few thermodynamic identities. Internal energy can be written in terms of specific free energy as:

$$e = \psi + \theta\eta \tag{91}$$

Therefore, the specific heat is given as (using (78)):

$$c_v = \left[\frac{\partial(\psi+\theta\eta)}{\partial\theta}\right]_v = \left(\frac{\partial\psi}{\partial\theta}\right)_v + \eta + \theta\left(\frac{\partial\eta}{\partial\theta}\right)_v \tag{92}$$

Using the definition of entropy from equation (86), equation (92) can be re-written as:

$$c_v = -\theta\frac{\partial^2\psi}{\partial\theta^2} \tag{93}$$

Substituting the definition of entropy from equation (86) into equation (80),

$$\Gamma c_v = -v\frac{\partial^2\psi}{\partial\theta\partial v} \tag{94}$$

Using relations in (93) and (94), the compatibility condition in equation (90) takes the following form.

$$v\frac{\partial c_v}{\partial v} = \theta\frac{\partial(\Gamma c_v)}{\partial\theta} \tag{95}$$

Equation (95) is called the compatibility condition and relates specific heat to the Gruneisen coefficient.

Using the compatibility condition, the third term in the expression for pressure in (89) can be simplified.

$$\int_{\theta_0}^{\theta} \frac{(\theta-\theta')}{\theta'} \frac{\partial c_v(v,\theta')}{\partial v} d\theta' = \int_{\theta_0}^{\theta} \frac{(\theta-\theta')}{v} \frac{\partial [\Gamma(v,\theta') c_v(v,\theta')]}{\partial \theta'} d\theta' \tag{96}$$

Apply integration by parts to equation (96),

$$\begin{aligned} &\int_{\theta_0}^{\theta} \frac{(\theta-\theta')}{\theta'} \frac{\partial c_v(v,\theta')}{\partial v} d\theta' \\ &= \left\{ \frac{(\theta-\theta')}{v} \Gamma(v,\theta') c_v(v,\theta') \right\}_{\theta_0}^{\theta} + \int_{\theta_0}^{\theta} \frac{\Gamma(v,\theta') c_v(v,\theta')}{v} d\theta' \\ &= -(\theta-\theta_0) \frac{\Gamma(v,\theta_0) c_v(v,\theta_0)}{v} + \int_{\theta_0}^{\theta} \frac{\Gamma(v,\theta') c_v(v,\theta')}{v} d\theta' \end{aligned} \tag{97}$$

Substitute (97) into equation (89) to get a simplified form for pressure:

$$P(v,\theta) = P(v,\theta_0) + \frac{1}{v} \int_{\theta_0}^{\theta} \Gamma(v,\theta') c_v(v,\theta') \, d\theta' \tag{98}$$

Equation (98) is called the complete equation of state and has been obtained without any assumptions so far. To find pressure from this relation, knowledge of the following three items is required:

(1) Isotherm at θ_0, i.e. $P(v,\theta_0)$
(2) Gruneisen parameter, $\Gamma(v,\theta)$
(3) Specific heat, $c_v(v,\theta)$

Equation (98) can be further simplified if we make an assumption on the form of Gruneisen parameter, $\Gamma(v,T)$. Let us assume that the Gruneisen parameter is a function of specific volume only, $\Gamma = \Gamma(v)$. For such a class of materials, the compatibility relation in (95) can be written as a hyperbolic partial differential equation in c_v:

$$v \frac{\partial c_v}{\partial v} = \theta \Gamma(v) \frac{\partial c_v}{\partial \theta} \tag{99}$$

Therefore, the characteristic curves for the above PDE are a solution to the following ODE:

$$\frac{d\theta}{dv} = -\frac{\Gamma(v)\theta}{v} \tag{100}$$

The characteristic curve that passes through the initial state (v_0,θ_0) is $\theta = \theta_0 \phi(v)$ and corresponds to an isentrope (shown in the isentrope section below), where the integrating factor, $\phi(v)$ is given as:

$$\phi(v) = \exp\left(-\int_{v_0}^{v} \frac{\Gamma(v')}{v'} dv' \right) \tag{101}$$

Specific heat capacity is constant along the characteristic curve, i.e.

$$c_v(v,\theta) = c_v(v_0,\theta_0) = c_v\left(v_0, \frac{\theta}{\phi(v)}\right) = \widetilde{c_v}\left(\frac{\theta}{\phi(v)}\right) = \widetilde{c_v}(\tilde{\theta}) \tag{102}$$

where the tilde signifies the scaled temperature, $\tilde{\theta} = \frac{\theta}{\phi(v)}$. Hence, for the class of materials with $\Gamma = \Gamma(v)$, specific heat is a function of single scaled temperature. Therefore, a further simplified form of pressure can be written as:

$$P(v,\theta) = P(v,\theta_0) + \frac{\Gamma(v)\phi(v)}{v}\int_{\tilde{\theta}_0}^{\tilde{\theta}} \tilde{c_v}(\tilde{\theta}')\, d\tilde{\theta}' \tag{103}$$

The derivative of the integrating factor in equation (102) is:

$$\frac{d\phi(v)}{dv} = -\frac{\phi(v)\Gamma(v)}{v} \tag{104}$$

Substituting (104) into (103),

$$P(v,\theta) = P(v,\theta_0) - \frac{d\phi(v)}{dv}\int_{\tilde{\theta}_0}^{\tilde{\theta}} \tilde{c_v}(\tilde{\theta}')\, d\tilde{\theta}' \tag{105}$$

We derive expressions for other thermodynamic quantities for the case of $\Gamma = \Gamma(v)$. Entropy can be re-written using equation (83):

$$\eta(v,\theta) = \eta_0 + \int_{v_0}^{v} \frac{\Gamma(v')\tilde{c_v}(\tilde{\theta}_0)}{v'} dv' + \int_{\tilde{\theta}_0}^{\tilde{\theta}} \frac{\tilde{c_v}(\tilde{\theta}')}{\tilde{\theta}'} d\tilde{\theta}' \tag{106}$$

Now, the expressions for Helmholtz specific free energy and specific internal energy can be simplified to the following relations:

$$\psi(v,\theta) = \psi_0 - \eta_0(\theta-\theta_0) - \int_{v_0}^{v}\left[P(v',\theta_0) + (\theta-\theta_0)\frac{\Gamma(v')\tilde{c}_v(\tilde{\theta}_0)}{v'}\right] dv' - \phi(v)\int_{\tilde{\theta}_0}^{\tilde{\theta}} \frac{(\tilde{\theta}-\tilde{\theta}')}{\tilde{\theta}'}\tilde{c}_v(\tilde{\theta}')d\tilde{\theta}' \tag{107}$$

$$\begin{aligned} e(v,\theta) &= \psi(v,\theta) + \theta\eta(v,\theta) \\ &= e_0 - \int_{v_0}^{v}\left[P(v',\theta_0) - \theta_0\frac{\Gamma(\mathrm{v}')\tilde{c_v}(\tilde{\theta}_0)}{v'}\right] dv' + \int_{\tilde{\theta}_0}^{\tilde{\theta}} \tilde{c_v}(\tilde{\theta}')\, d\tilde{\theta}' \end{aligned} \tag{108}$$

where $e_0 = \psi_0 + \theta_0\eta_0$.

At this juncture, it is worth noting that if $T_0 = 0K$ is chosen as the reference temperature, specific heat and entropy go to zero, i.e. $c_v(v,T_0) \to 0$ and $\eta_0 = 0$. The expressions above then simplify to:

$$P(v,\theta) = P_c(v) - \frac{d\phi(v)}{dv}\int_{0}^{\tilde{\theta}} \tilde{c_v}(\tilde{\theta}')\, d\tilde{\theta}' \tag{109}$$

$$\eta(v,\theta) = \int_{0}^{\tilde{\theta}} \frac{\tilde{c_v}(\tilde{\theta}')}{\tilde{\theta}'} d\tilde{\theta}' \tag{110}$$

$$\psi(v,\theta) = \psi_0 - \int_{v_0}^{v} P_c(v')dv' - \phi(v)\int_{0}^{\tilde{\theta}} \frac{(\tilde{\theta}-\tilde{\theta}')}{\tilde{\theta}'}\tilde{c}_v(\tilde{\theta}')d\tilde{\theta}' \tag{111}$$

$$e(v,\theta) = e_0 - \int_{v_0}^{v} P_c(v')dv' + \int_{0}^{\tilde{\theta}} \tilde{c_v}(\tilde{\theta}')\, d\tilde{\theta}' \tag{112}$$

Even though using the cold curve isotherm makes the expressions for thermodynamic entities compact, we prefer to use relations in (105)-(108) for ease of obtaining material properties at temperatures other than the absolute zero.

THERMOELASTIC HEATING

Specify role of thermo-elastic heating and why its derivation in this section could be of potential interest. In section 2.5, it was shown that the rate of heat generation due to elastic processes is given as:

$$\dot{q}^e = \left(\frac{\theta}{2}\frac{\partial \boldsymbol{T^e}}{\partial \theta} : \dot{\boldsymbol{C}}^{\boldsymbol{e}}\right) \tag{113}$$

The above relation can be written in terms of Mandel stress:

$$\dot{q}^e = \frac{\theta}{2}\,\boldsymbol{C^{e-1}}\,\frac{\partial \boldsymbol{M^e}}{\partial \theta} : \dot{\boldsymbol{C}}^{\boldsymbol{e}} = \frac{\theta}{2}\,\frac{\partial \boldsymbol{M^e}}{\partial \theta} : \boldsymbol{C^{e-T}}\dot{\boldsymbol{C}}^{\boldsymbol{e}} \tag{114}$$

From equation (56), the derivative of Mandel stress with respect to temperature can be calculated as:

$$\frac{\partial \boldsymbol{M^e}}{\partial \theta} = -\frac{\partial P}{\partial \theta} J^e \boldsymbol{I} + 2\frac{\partial G}{\partial \theta}\boldsymbol{E_0^e} \tag{115}$$

Let us consider writing the right Cauchy-Green tensor in the right principal basis, $(\boldsymbol{r_1^e}\otimes\boldsymbol{r_1^e}, \boldsymbol{r_2^e}\otimes\boldsymbol{r_2^e}, \boldsymbol{r_3^e}\otimes\boldsymbol{r_3^e})$ in terms of right elastic stretches, $(\lambda_1^e, \lambda_2^e, \lambda_3^e)$.

$$\boldsymbol{C^e} = \sum_{i=1}^{3} (\lambda_i^e)^2\, \boldsymbol{r_i^e}\otimes\boldsymbol{r_i^e} \tag{116}$$

The term $\boldsymbol{C^{e-T}}\dot{\boldsymbol{C}}^{\boldsymbol{e}}$ in equation (114) can then be simplified as:

$$\boldsymbol{C^{e-T}}\dot{\boldsymbol{C}}^{\boldsymbol{e}} = \sum_{i=1}^{3} \frac{2\dot{\lambda_i^e}}{\lambda_i^e}\, \boldsymbol{r_i^e}\otimes\boldsymbol{r_i^e} \tag{117}$$

Similarly, the deviatoric part of elastic logarithmic strain tensor can be expressed in the right principal basis:

$$\boldsymbol{E_0^e} = \boldsymbol{E^e} - \frac{tr(\boldsymbol{E^e})}{3}\boldsymbol{I} = \sum_{i=1}^{3} \ln(\lambda_i^e)\, \boldsymbol{r_i^e}\otimes\boldsymbol{r_i^e} - \frac{\ln(J^e)}{3}\boldsymbol{I} \tag{118}$$

Thus, from equations (114), (115), (117) and (118), thermoelastic heating can be written in matrix form as:

$$\begin{aligned}\dot{q}^e = \theta\frac{\partial G}{\partial \theta}&\begin{bmatrix} \ln\left[\frac{\lambda_1^e}{(J^e)^{1/3}}\right] & 0 & 0 \\ 0 & \ln\left[\frac{\lambda_2^e}{(J^e)^{1/3}}\right] & 0 \\ 0 & 0 & \ln\left[\frac{\lambda_3^e}{(J^e)^{1/3}}\right] \end{bmatrix} : \begin{bmatrix} 2\frac{\dot{\lambda_1^e}}{\lambda_1^e} & 0 & 0 \\ 0 & 2\frac{\dot{\lambda_2^e}}{\lambda_2^e} & 0 \\ 0 & 0 & 2\frac{\dot{\lambda_3^e}}{\lambda_3^e} \end{bmatrix} \\ &- \frac{\theta}{2}\frac{\partial P}{\partial \theta} J^e \begin{bmatrix} 1 & 0 & 0 \\ 0 & 1 & 0 \\ 0 & 0 & 1 \end{bmatrix} : \begin{bmatrix} 2\frac{\dot{\lambda_1^e}}{\lambda_1^e} & 0 & 0 \\ 0 & 2\frac{\dot{\lambda_2^e}}{\lambda_2^e} & 0 \\ 0 & 0 & 2\frac{\dot{\lambda_3^e}}{\lambda_3^e} \end{bmatrix}\end{aligned} \tag{119}$$

$$\Longrightarrow \dot{q}^e = \theta \frac{\partial G}{\partial \theta} \sum_{i=1}^{3} \ln\left[\frac{\lambda_i^e}{(J^e)^{\frac{1}{3}}}\right]\left(2\frac{\dot{\lambda_i^e}}{\lambda_i^e}\right) - \frac{\theta}{2}\frac{\partial P}{\partial \theta} J^e \sum_{i=1}^{3}\left(2\frac{\dot{\lambda_i^e}}{\lambda_i^e}\right) \tag{120}$$

Since $J^e = \lambda_1^e \lambda_2^e \lambda_3^e$ and hence, $\frac{\dot{J^e}}{J^e} = \sum_{i=1}^{3} \frac{\dot{\lambda_i^e}}{\lambda_i^e}$, we have:

$$\dot{q}^e = \theta \frac{\partial G}{\partial \theta} \sum_{i=1}^{3} \ln\left[\frac{\lambda_i^e}{(J^e)^{\frac{1}{3}}}\right]\left(2\frac{\dot{\lambda_i^e}}{\lambda_i^e}\right) - \theta \frac{\partial P}{\partial \theta} \dot{J^e} \tag{121}$$

While the second term in equation (121) is easy to compute from the complete equation of state form, the first term is tedious and requires knowledge of principal elastic stretches and stretch rates in all 3 principal directions. However, if the dependence of shear modulus on temperature is negligible, the expression for thermoelastic heating simplifies significantly. From sucrose simulations, we can try to compare the contribution of each of these terms to thermoelastic heating and also draw a comparison between thermoelastic heating and thermo-viscoplastic heating.

In the next few sections, analytic expressions for different thermodynamic curves like the isentrope, isotherm and Hugoniot are derived using the complete equation of state. Plotting these curves for sucrose is expected to provide insights into material behavior under different types of loading.

ISENTROPE

The loading under pressure-shear plate impact can be considered as the closest to an isentrope, i.e. the PSPI experiments load the specimen quasi-entropically. Pressure along an isentrope can be found using Mie-Gruneisen EOS in (66) in terms of the reference curve:

$$P^{(\eta)}(v) - P^{ref}(v) = \frac{\Gamma(v)}{v}\left[e^{(\eta)}(v) - e^{ref}(v)\right] \tag{122}$$

where the superscript η specifies quantities along the isentrope. However, the specific internal energy, $e^{(\eta)}(v)$ remains unknown. If $e = e(v, \eta)$, pressure is defined as (equation (72)):

$$P(v, \eta) \equiv -\left(\frac{\partial e}{\partial v}\right)_{\eta} = -\frac{de^{(\eta)}}{dv} \tag{123}$$

Substitute (123) into (122) to obtain an ODE in $e^{(\eta)}(v)$:

$$\frac{de^{(\eta)}(v)}{dv} + \frac{\Gamma(v)}{v} e^{(\eta)}(v) = -\left[P^{ref}(v) - \frac{\Gamma(v)}{v} e^{ref}(v)\right] \tag{124}$$

Using the integrating factor $\phi(v)$ defined in equation (101), the ODE can be written as:

$$\frac{d}{dv}\left(\frac{e^{(\eta)}(v)}{\phi(v)}\right) = -\frac{1}{\phi(v)}\left[P^{ref}(v) - \frac{\Gamma(v)}{v} e^{ref}(v)\right] \tag{125}$$

So, the internal energy associated with an isentrope passing through the initial state (v_0, e_0) is given as:

$$e^{(\eta)}(v) = \phi(v)\left\{e_0 - \int_{v_0}^{v} \frac{1}{\phi(v')}\left[P^{ref}(v') - \frac{\Gamma(v')}{v'} e^{ref}(v')\right] dv'\right\} \tag{126}$$

Substituting the above expression for specific internal energy into equation (126), expression for pressure along an isentrope can be obtained.

Variation of temperature during mechanical loading is imperative to an accurate and complete description of constitutive behavior of a material. Hence, calculating temperature changes during an isentropic loading is of prime interest. This can be achieved by considering an alternative definition of the Gruneisen parameter:

$$\Gamma \equiv v\left(\frac{\partial P}{\partial e}\right)_v = -\frac{v}{\theta}\left(\frac{\partial \theta}{\partial v}\right)_\eta \tag{127}$$

The second relation in (127) can be obtained from equations (78) and (80). Integrating, the temperature along an isentrope can be obtained.

$$\theta^{(\eta)} = \theta_0 \exp\left(-\int_{v_0}^{v} \frac{\Gamma(v')}{v'} dv'\right) = \theta_0 \phi(v) \tag{128}$$

Since (128) represents a characteristic curve for the hyperbolic PDE in (99), it implies that $c_v = constant$ along any isentrope. Isentrope for sucrose is plotted in 10. Note that the material properties for sucrose are discussed in the last section of the chapter.

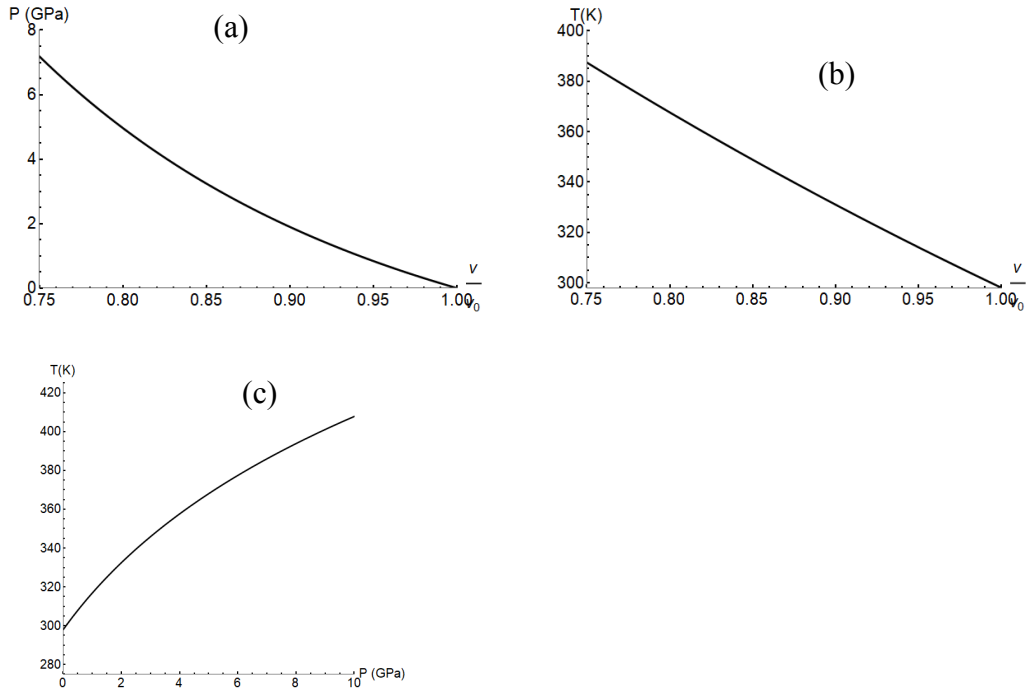

Figure 10 Isentrope curves for sucrose. Initial state is characterized by $v_0 = 1/\rho_0$, $P_0 = 0$, $T_0 = 298\ K$ and $e_0 = 0$, where ρ_0 is the initial density of sucrose.

ISOTHERM

Pressure along an isotherm can be obtained from equation (105) by substituting the isotherm temperature, $\theta = \theta_i$.

$$P(v, \theta_i) = P(v, \theta_0) - \frac{d\phi(v)}{dv} \int_{\tilde{\theta}_0}^{\tilde{\theta}_i} \tilde{c_v}\left(\tilde{\theta}'\right) d\tilde{\theta}' \tag{129}$$

Similarly, the expressions for specific internal energy, specific free energy and specific entropy can be obtained by substituting the isotherm temperature in (106)-(108). The curves below show isotherms for sucrose at different temperatures. A 3rd order Birch-Murnaghan equation of state is

chosen as the reference isotherm. The derivation of this equation of state is presented in section 10.

$$P = K_{\theta 0}\left(\frac{v_0}{v}\right)\ln\left(\frac{v_0}{v}\right)\left[1 + \frac{K'_{\theta 0} - 2}{2}\ln\left(\frac{v_0}{v}\right)\right] \tag{130}$$

where $K_{\theta 0}$ and $K'_{\theta 0}$ are elastic bulk modulus and the first derivative of elastic bulk modulus with respect to pressure. 11 shows isotherms for sucrose at different temperatures.

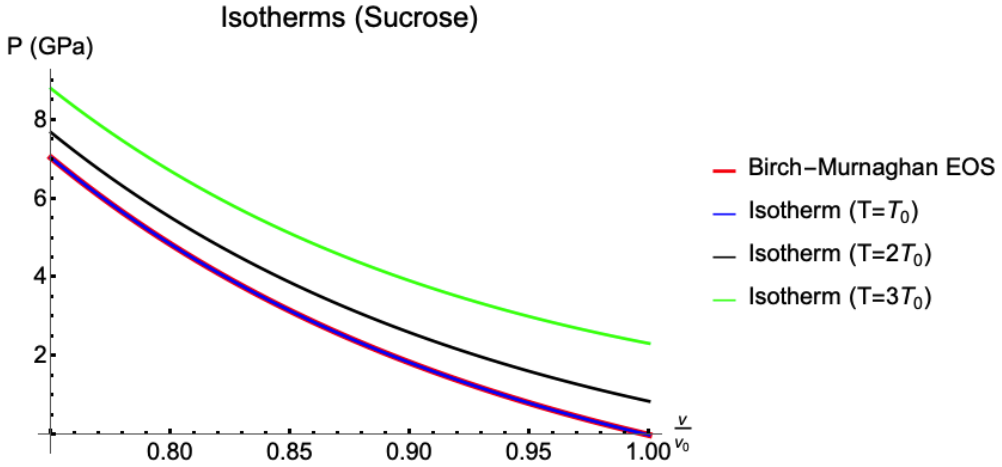

Figure 11 Isotherms for sucrose at different temperatures. $\theta_0 = 298\ K$.

HUGONIOT

Consider the case of a shock wave traveling through a solid so that high pressures are achieved. Under such high pressures, the shear strength of the solid is negligible with respect to the pressure applied. So, the normal stress jump across the shock wave can be equated to the pressure jump. Then, the specific internal energy of the solid for shock compression from an initial state of $(e_0, P_0, \theta_0, v_0)$ is given through the following Rankine-Hugoniot relation:

$$e^{(H)}(v) = e_0 + \frac{1}{2}\left(P^{(H)}(v) + P_0\right)(v_0 - v) \tag{131}$$

Pressure along a Hugoniot requires another piece of information. Usually, that is provided in terms of a shock speed-particle speed relation (example $u_s = c_0 + su_p$). Another way to find the pressure on a Hugoniot is by using a reference curve and then substituting into the Mie-Gruneisen equation of state. We choose to go ahead with the latter to be consistent with the above formulation.

$$P^{(H)}(v) - P(v, \theta_0) = \frac{\Gamma(v)}{v}\left[e^{(H)}(v) - e(v, \theta_0)\right] \tag{132}$$

Internal energy along an isotherm can be found from equation (108):

$$e(v, \theta_0) = e_0 - \int_{v_0}^{v}\left[P(v', \theta_0) - \theta_0\frac{\Gamma(\mathrm{v}')\tilde{c_v}\left(\tilde{\theta}_0\right)}{v'}\right]dv' \tag{133}$$

Substituting the expressions for internal energy from (131) and (133) into equation (132), pressure along a Hugoniot can be written as:

$$P^{(H)}(v) = \frac{\frac{\Gamma(v)}{v}P_0(v_0 - v) + P(v,\theta_0) + \frac{\Gamma(v)}{v}\left\{\int_{v_0}^{v}\left[P(v',\theta_0) - \theta_0\frac{\Gamma(v')\widetilde{c_v}(\widetilde{\theta_0})}{v'}\right]dv'\right\}}{1 - \frac{\Gamma(v)}{2v}(v_0 - v)} \tag{134}$$

Now, we turn our attention to finding the temperature change along a Hugoniot. Consider internal energy as a function of volume and entropy, $e(v,\eta)$. Change in internal energy can be written using the first law of Thermodynamics (equation (70)) as $de = -Pdv + \theta d\eta$. Consider $\eta = \eta(v,\theta)$. From equation (82), change in entropy can be written as $d\eta = \frac{\Gamma c_v}{v}dv + \frac{c_v}{\theta}d\theta$. Hence, the first law of thermodynamics is

$$de = \left(-P + \frac{\Gamma c_v \theta}{v}\right)dv + c_v d\theta \tag{135}$$

In a differential form, equation (135) can be written as:

$$de^{(H)} = \frac{1}{2}(v_0 - v)dP^{(H)} - \frac{1}{2}\left(P^{(H)} + P_0\right)dv \tag{136}$$

Equating right hand sides of equations (135) and (136):

$$\left(-P^{(H)} + \frac{\Gamma c_v \theta^{(H)}}{v}\right)dv + c_v d\theta^{(H)} = \frac{1}{2}(v_0 - v)dP^{(H)} - \frac{1}{2}\left(P^{(H)} + P_0\right)dv \tag{137}$$

Rearranging, we get a first-order ODE in $\theta^{(H)}$,

$$c_v\frac{d\theta^{(H)}}{dv} + \frac{\Gamma c_v}{v}\,\theta^{(H)} = \underbrace{\frac{1}{2}(v_0 - v)\frac{dP^{(H)}(v)}{dv} + \frac{1}{2}\left(P^{(H)}(v) - P_0\right)}_{h(v)} \tag{138}$$

The right hand side of (138) is a function of specific volume and can be abbreviated into a function $f(v)$. $P^{(H)}$ can be substituted from equation (134). Consider the derivative of scaled temperature, $\tilde{\theta} = \theta/\phi(v)$, with respect to v:

$$\phi(v)\frac{d\tilde{\theta}}{dv} = \frac{d\theta}{dv} + \frac{\Gamma(v)}{v}\theta \tag{139}$$

Substitute (139) into (138):

$$\widetilde{c_v}\left(\tilde{\theta}^{(H)}\right)\frac{d\tilde{\theta}^{(H)}}{dv} = \frac{h(v)}{\phi(v)} \tag{140}$$

Equation (140) gives temperature change along a Hugoniot. In its most generic form, the temperature relation above is a non-linear ODE and needs to be solved using numerical methods. The special case of a constant specific heat can be solved easily. Hugoniot curves for sucrose are shown in 12.

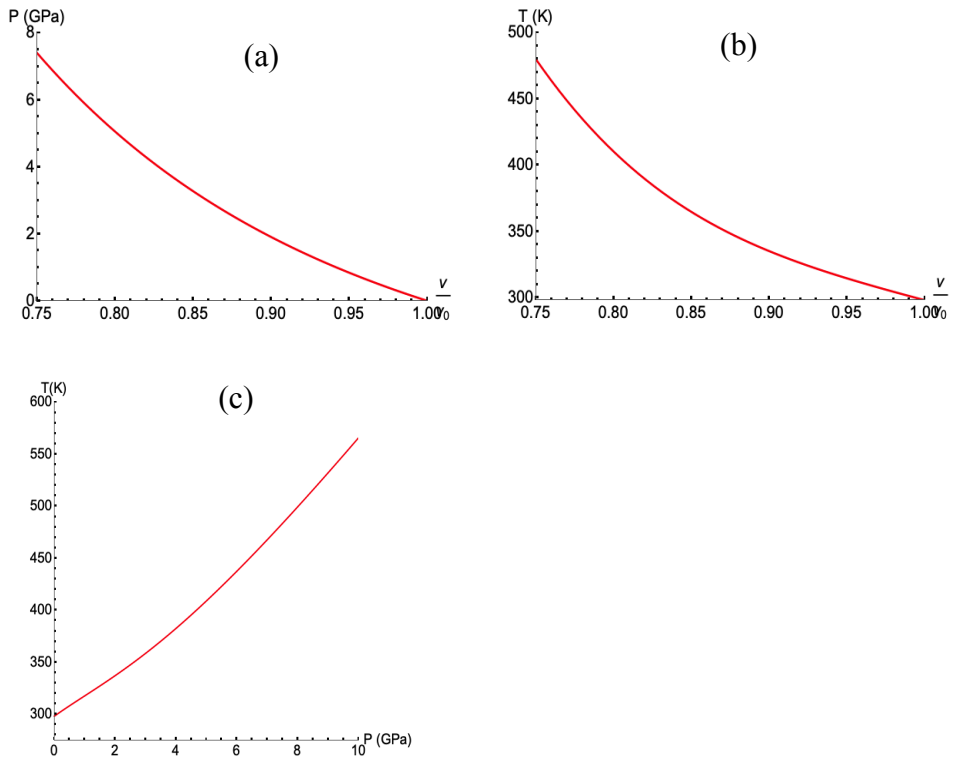

Figure 12 Hugoniot curves for sucrose.

COMPARISON OF THERMODYNAMIC CURVES

At this point, it is instructive to compare the pressure-volume-temperature (P, v, θ) response under different types of commonly encountered loading. 13 shows a three-dimensional surface of a complete Mie-Gruneisen equation of state for sucrose in the (P, v, θ) space. An isotherm, an isentrope and a Hugoniot are plotted simultaneously. 13 clearly illustrates the vast difference between the three curves along the temperature axis. For more illustrative comparisons, we compare the thermodynamic curves on two-dimensional plots. Figure 14 shows that in the pressure, P vs compression ratio, v/v_0 ratio, the Hugoniot lies above the isentrope while the isotherm lies at the bottom of the three curves. However, for the volume compression ratios considered here, the difference between the curves is negligible. The main difference between the isotherm, isentrope and Hugoniot lies in the temperature response of the material, as shown in Figure 15 and Figure 16. While the temperature rise along an isentrope is almost linear with volume compression ratio, temperature along the Hugoniot quickly diverges from the isentrope and leads to a much quicker temperature rise. It is to be noted that while the temperature rise along an isentrope slows down with increasing pressure (Figure 16), the temperature rise along a Hugoniot quickens with increasing pressure as indicated by the concave up curve. These differences in the material response to different types of thermodynamic loading has far reaching consequences for explosives. For example, a ramp wave with an isentropic pressure loading is much less likely to cause hot spots as compared to a shock wave.

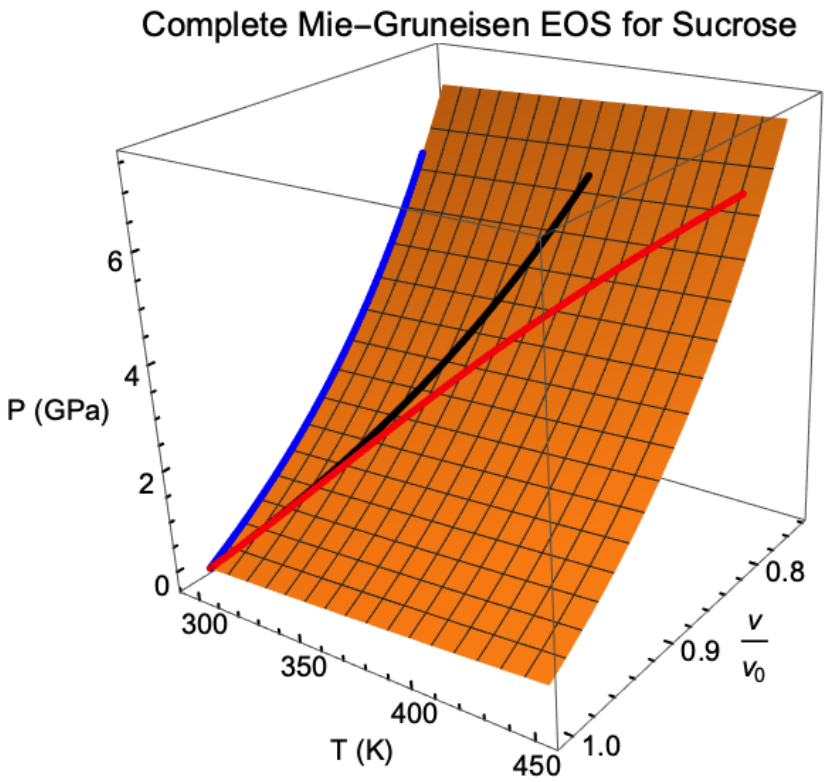

Figure 13. Pressure-Volume-Temperature curve for a complete Mie-Gruneisen equation of state for sucrose (Orange grid). Blue: Isotherm, Black: Isentrope and Red: Hugoniot, all passing through the initial state, $P_0 = 0, v_0, \theta_0 = 298K$.

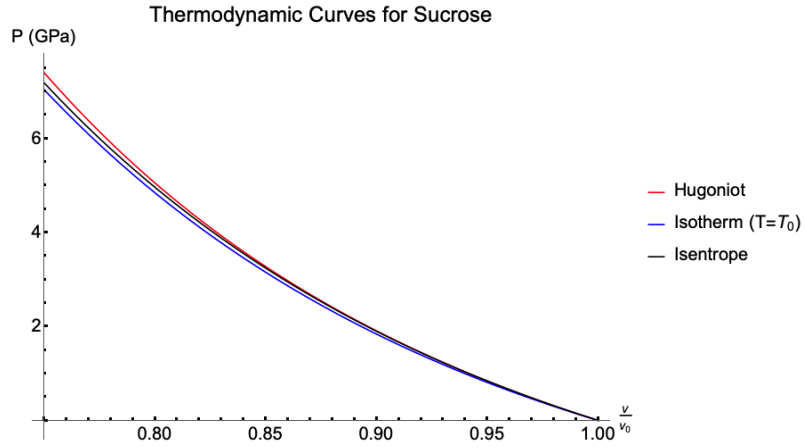

Figure 14. Pressure, P vs compression ratio, v/v_0 plots for sucrose, for a Hugoniot, an isentrope and an isotherm, all passing through the same initial point, i.e. $P_0 = 0, \frac{v}{v_0} = 1, \theta_0 = 298\ K$

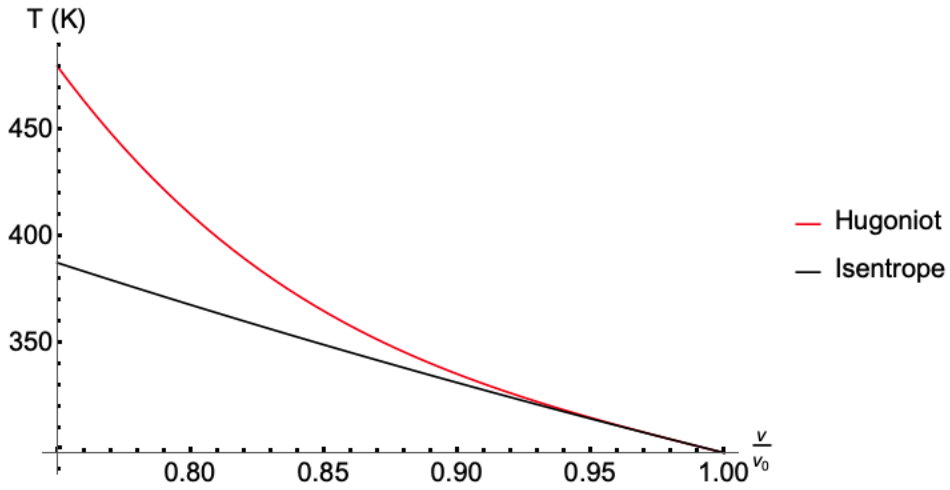

Figure 15. Temperature, θ vs compression ratio, v/v_0 plots for sucrose, for a Hugoniot and an isentrope

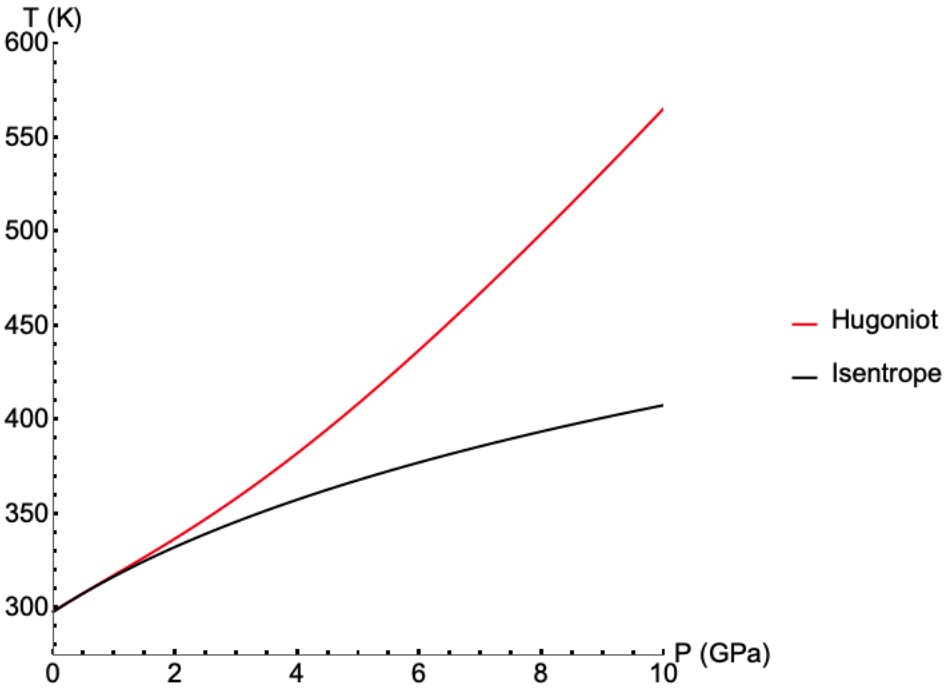

Figure 16. Temperature, θ vs pressure, P plots for sucrose, for a Hugoniot and an isentrope

At this point, it is also imperative to discuss the importance of using a complete equation of state with a temperature dependent specific heat capacity. As noted by Menikoff and Sewell (*Combustion Theory and Modelling,* 6**,** 103-125, 2002), incorporating temperature dependence of specific heat in an equation of state is extremely important to accurately predict hot-spot temperatures and hence the consequent chemical reaction kinetics. Let us compare the thermodynamic response of sucrose for two cases: (a) Temperature dependent specific heat capacity, and (b) Constant specific heat capacity, evaluated at $\theta = \theta_0$.

Figure 17 shows the differences arising in the temperature response due to the form of specific heat chosen. As expected, the temperature along the isentrope should be unaffected by the choice of specific heat capacity because the specific heat capacity remains constant along an isentrope. However, there is a huge difference in the temperature rise along a Hugoniot. Using the temperature-dependent specific heat, $c_v(\theta)$ results in a lower temperature increase with compression as compared to using a constant specific heat, $c_v(\theta_0)$, with the difference between the two cases increasing as the compression ratio increases. Such a comparison emphasizes the role played by the choice of specific heat capacity for shock wave loading of explosive/simulant crystals. This choice has consequences for accurately simulating the mechanical, thermal and chemical response of energetic materials. For example, the comparison of Hugoniots with the pressure-dependent melt curve for sucrose shows that beyond a compression ratio of ~0.67, Hugoniot with a constant specific heat capacity predicts melting while using a complete equation of state does not. This has a significant impact on predicting mechanical localization and the formation of features like adiabatic shear bands, which further affect formation of hot-spots and the probability with which hot-spots turn critical leading to an unsustained chemical reaction and eventually a detonation wave. To conclude, simulations using a constant specific heat might yield very different results from those predicted by a complete equation of state. This underlines the importance of developing a complete equation of state for sucrose. Such a framework can now be directly utilized for explosive crystals like HMX and RDX.

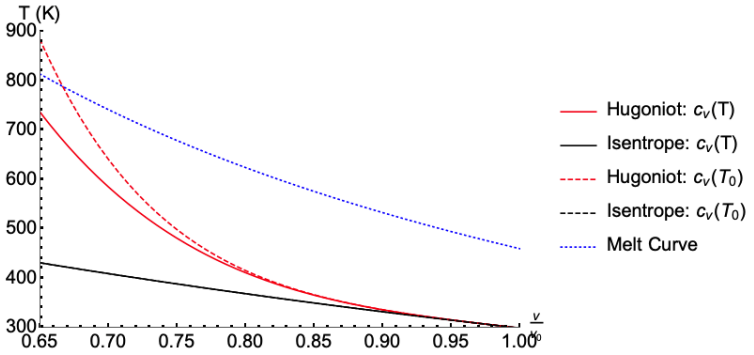

Figure 17 Effect of specific heat capacity on temperature rise along a Hugoniot and an isentrope with increasing compression, for sucrose. The pressure-dependent melt curve for sucrose is also shown

At this juncture, one may pose a question: If a constant specific heat were to be used for simplicity, in a material model for sucrose, at what temperature should it be evaluated? To answer this question, we plot the temperature along a Hugoniot for constant specific heat (dashed curves) at different temperatures and compare with the case of temperature-dependent specific heat (solid curve). From Figure 18, it becomes clear that for the range of pressures considered, $c_v = 1.5\ c_{v0}$ works the best.

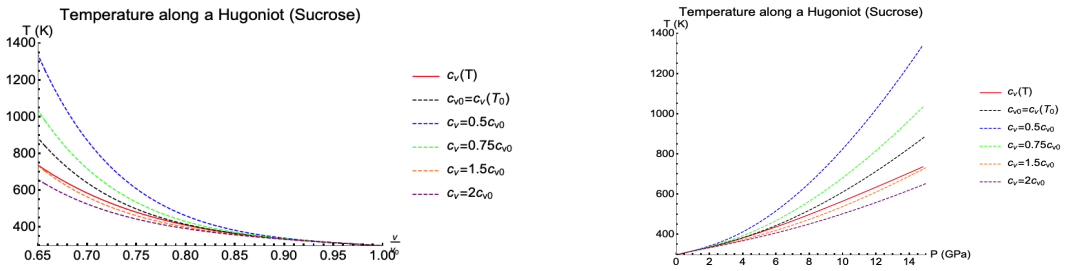

Figure 18. Temperature along a Hugoniot for sucrose for different specific heat capacities.

DERIVATION OF 3RD ORDER BIRCH-MURNAGHAN EQUATION OF STATE

A 3rd order free-energy function is used to derive an isothermal equation of state. Note that the final form of equation of state depends on the strain measure used. The $P - v$ relation based on the Euler-Almansi strain is the most commonly encountered form in shock physics and geophysics applications and is as follows:

$$P = \frac{3}{2}K_{T0}\left[\left(\frac{v_0}{v}\right)^{\frac{7}{3}} - \left(\frac{v_0}{v}\right)^{\frac{5}{3}}\right]\left[1 + \frac{3}{4}(K'_{T0} - 4)\left\{\left(\frac{v_0}{v}\right)^{\frac{2}{3}} - 1\right\}\right] \tag{141}$$

However, since the constitutive model is built using logarithmic strains, it is important to be consistent and use the same strain measure.

Consider a cube of an isotropic material subjected to pressure. The deformation gradient for such a deformation is given below:

$$\boldsymbol{F} = \lambda \boldsymbol{I} \tag{142}$$

Volumetric logarithmic strain is given as:

$$E_v = tr(\boldsymbol{E^e}) = \ln(\lambda^3) = \ln\left(\frac{v}{v_0}\right) \tag{143}$$

Now consider a polynomial expansion of Helmholtz free energy per unit volume in the reference configuration, as a function of magnitude of volumetric strain:

$$\psi_R(E^v) = A_0 + A_1E_v + A_2E_v^2 + A_3E_v^3 \ldots \tag{144}$$

Pressure inside the solid is given as:

$$P = -\frac{1}{\rho_0}\frac{\partial \psi_R}{\partial v} \tag{145}$$

Assume that the free energy and pressure are zero in the reference configuration, i.e. $A_0 = 0, A_1 = 0$. Then the expression for pressure can be simplified in terms of A_2 and A_3:

$$P = -\frac{1}{\rho_0}\frac{\partial \psi_R}{\partial v} = -\frac{1}{\rho_0}\frac{\partial \psi_R}{\partial E_v}\frac{\partial E_v}{\partial \lambda}\frac{\partial \lambda}{\partial v} = -E_v\left(\frac{2A_2 + 3A_3E_v}{\lambda^3}\right) \tag{146}$$

We wish to write the constants A_2 and A_3 in terms of measurable material parameters like the isothermal bulk modulus, $K_{\theta 0}$ and its first pressure derivative, $K'_{\theta 0}$. The subscript '0' refers to the reference state of $(v_0, P_0 = 0, \theta_0 = 298\ K)$. $K_{\theta 0}$ and $K'_{\theta 0}$ are defined below:

$$K_{\theta 0} = -v\frac{\partial P}{\partial v} \tag{147}$$

$$K'_{\theta 0} = \frac{\partial K_{\theta 0}}{\partial \theta} \tag{148}$$

Using equations (146), (147) and (148), we can find A_2 and A_3 in terms of $K_{\theta 0}$ and $K'_{\theta 0}$:

$$A_2 = \frac{K_{\theta 0}}{2} \tag{149}$$

$$A_3 = \frac{K_{\theta 0}}{6}(2 - K'_{\theta 0}) \tag{150}$$

Substituting the above relations into equation (146), the 3rd-order Birch-Murnaghan equation of state in terms of logarithmic strains is written as:

$$P = K_{\theta 0}\left(\frac{v_0}{v}\right)\ln\left(\frac{v_0}{v}\right)\left[1 + \frac{K'_{\theta 0} - 2}{2}\ln\left(\frac{v_0}{v}\right)\right] \tag{151}$$

A comparison of the 3rd order Birch-Murnaghan EOS using the 3 different strain measures is shown in the plot below (Figure 19). It is evident that the Green-Lagrange strain leads to the most compliant behavior at the same volumetric compression while the Euler-Almansi form leads to the stiffest behavior. The Birch-Murnaghan forms for the logarithmic strain and Euler-Almansi strain are in extremely close approximation of each other even for finite volumetric strains. All the 3 forms show excellent agreement at small strains which is to be expected.

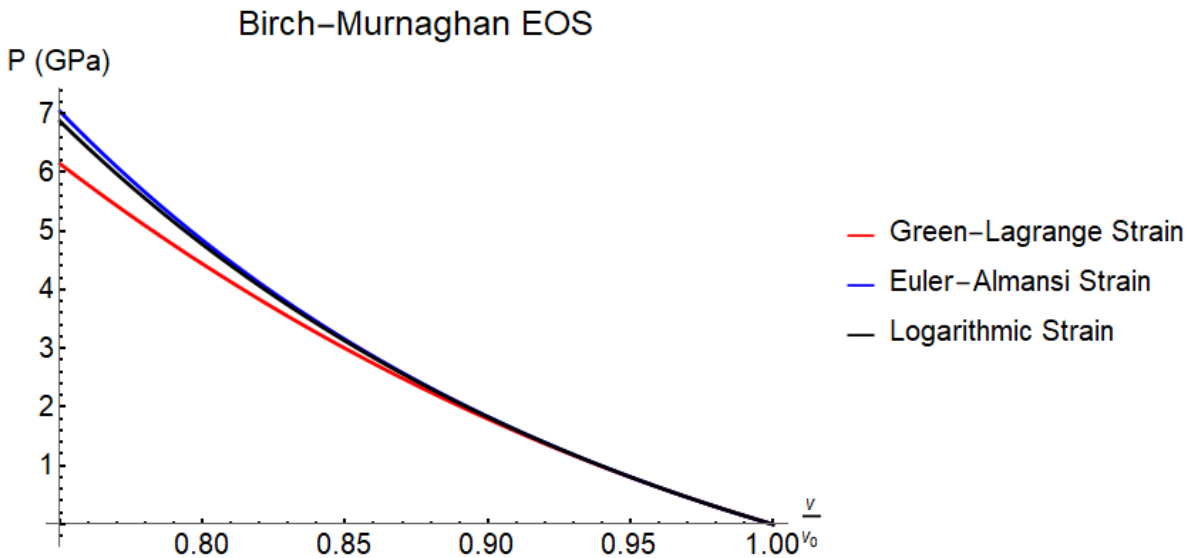

Figure 19. 3rd order Birch-Murnaghan equation of state using 3 different strain measures

MATERIAL PROPERTIES OF SUCROSE

Elastic Constants

Bulk Modulus

Bridgman made measurements of compression ratios of sucrose under pressures up to 3 GPa (see Table V in (Bridgman 1949)). The bulk modulus and elastic modulus (assuming Poisson's ratio, $\nu = 0.25$) are shown in the table below:

Table 1 Elastic moduli of sucrose measured at different pressures. Bulk moduli and volumetric changes are calculated based on Table V in (Bridgman 1949).

Pressure (kg/cm^2)	Pressure (GPa)	$\frac{\Delta V}{V_0}$	Bulk Modulus, K (GPa)	Young's Modulus, $E = 3K(1-2\nu), \nu = 0.25$	Shear Modulus $\mu = \frac{E}{2(1+\nu)}$
5,000	**0.5**	**0.03151**	**15.868**	**23.802**	**9.521**
10,000	1	0.05518	18.122	27.184	10.873
15,000	1.5	0.07434	20.178	30.266	12.107
20,000	2	0.09074	22.041	33.061	13.225
25,000	2.5	0.10552	23.692	35.538	14.215
30,000	3	0.11866	25.282	37.923	15.169

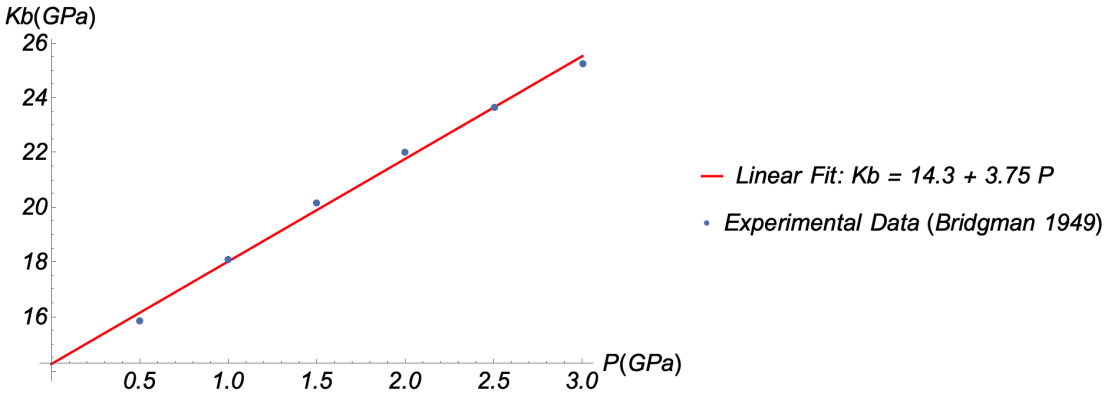

Figure 20. Linear fit to experimental data for bulk modulus of sucrose

Figure 20 indicates the pressure dependence of bulk modulus for sucrose. $K_{T0} = 14.3\ GPa$ and $K'_{T0} = 3.75$ are obtained using a linear fit to the experimental data. K_{T0} is the isothermal bulk modulus at ambient temperature and pressure while K'_{T0} is the first derivative of bulk modulus with respect to pressure at ambient temperature and pressure. These values are very close to the data obtained from (Bridgman 1933).

Poisson's Ratio and Young's Modulus

(Trott et al. 2007) use a Poisson's ratio of 0.25 for sucrose. Using $K_{T0} = 14.3\ GPa$ and $\nu = 0.25$, $E = 21.45\ GPa$ is obtained.

Thermal Constants

Coefficient of Thermal Expansion

A mean volumetric coefficient of thermal expansion of $140.1 \times 10^{-6}\ ^{\circ}\mathrm{C}^{-1}$ is reported by (Bridgman 1933) over a temperature range of $30\ ^{0}C$ to $75\ ^{0}C$.

Specific Heat

Specific heat capacity at constant pressure, c_p is reported by (Anderson Jr, Higbie and Stegeman 1950) over a temperature range of $25\ ^{0}C$ to $90\ ^{0}C$. The experimental data is given in Table 2. In order to derive specific heat capacity at constant volume, c_v the following thermodynamic relation can be used:

$$c_p - c_v = vT\alpha^2 K_T \tag{152}$$

where $v = V/m$ is specific volume, α is the coefficient of thermal expansion and K_T is the isothermal Bulk Modulus. It can be noted that the difference in c_p and c_v values is extremely small.

Table 2 Specific heat capacities of sucrose. c_p values are direct experimental measurements while c_v values are derived from thermodynamic constraints

Temp (K)	$c_p\left(\frac{J}{kg\ K}\right)$ (Experimentally Measured)	$\boldsymbol{c_v}\ (= c_p - vT\alpha^2 K_T)$
275.6	1137.98	1087.331
281.9	1167.32	1115.513
289.7	1200.32	1147.079
296.2	1255.32	1200.885
296.8	1234.54	1179.995
296.9	1238.21	1183.646
299.4	1250.43	1195.407
301.2	1250.43	1195.076
302.8	1263.88	1208.232
313	1313.99	1256.467
320.3	1351.89	1293.026
342.4	1476.56	1413.634
362.7	1581.68	1515.024

Fitting to Debye Relation

Using a complete equation of state requires temperature dependent specific heat capacity. However, experimentally measured values are not available for the entire temperature range of interest. So, specific heat capacity is fit to the well-known Debye model of specific heat capacity.

$$c_v = \frac{9Nk}{M}\left(\frac{\theta}{\theta_D}\right)^3 \int_0^{\theta_D/\theta} \frac{x^4 e^x}{(e^x - 1)^2} dx = 3A\left(\frac{\theta}{\theta_D}\right)^3 \int_0^{\theta_D/\theta} \frac{x^4 e^x}{(e^x - 1)^2} dx \tag{153}$$

Where N is the number of atoms, k is the Boltzmann constant, M is the molecular mass, θ_D is Debye temperature and $A = \frac{3Nk}{M}$. At $\theta \to 0, c_v \to 0$ and $\theta \to \infty, c_v \to fR_0/M$ where the latter asymptotic limit is referred to as the Dulong-Petit limit. $R_0 = 8.314 \frac{J}{K\ mol}$ is the universal gas constant and M is the molecular mass in kg/mol. f represents the degrees of freedom contributing to specific heat. For a monoatomic molecule, $f = 3$. However, for complex polyatomic molecules like HMX and sucrose, the number of degrees of freedom is very large. For any non-linear molecule, the total degrees of freedom is $3N$ (3 translational, 3 rotational and 3N-6 vibrational) where N is the number of atoms in the molecule. Hence, the Dulong-Petit limit of specific heat should be $\theta \to \infty, c_v \to 3NR_0/M$. However, as is noted in Menikoff and Sewell (*Combustion Theory and Modelling,* 6**,** 103-125, 2002), some of the vibrational degrees of freedom corresponding to C-H bond stretching in HMX do not contribute to the specific heat capacity (as the vibrational frequencies of C-H bonds are very high and these modes are not very highly populated). Therefore, for HMX, the Dulong-Petit limit is expected to be $\theta \to \infty, c_v \to (3 \times 28 - 8)R_0/M$, where number of atoms in HMX is 28 and number of C-H bonds is 8. However, no such information is available about the vibrational frequencies C-H bonds in sucrose. So, to begin with, a conservative limit for specific heat of sucrose is assumed, i.e. as $\theta \to \infty, c_v \to \frac{135R_0}{M} = 3279 \frac{J}{kg\ K}$ $(M = 342.3\ g/mol)$.

Aside: Dulong-Petit limit for monoatomic solids specifies

$$\lim_{\theta \to \infty} c_{v,molar} = 3R_0 \tag{154}$$

where R_0 is the universal gas constant and the molar specific heat capacity, $c_{v,molar}$ is given below:

$$c_{v,molar} = \frac{C_v}{n} \tag{155}$$

where C_v is the heat capacity and $n = m/M$ is the number of moles, m is mass and M is molecular mass. However, the commonly used form of specific heat is defined below:

$$c_v = \frac{C_v}{m} = \frac{C_v}{n}\frac{1}{M} = \frac{c_{v,molar}}{M} \tag{156}$$

Hence, the Dulong-Petit limit can be re-written as:

$$\lim_{\theta \to \infty} c_v = \frac{3R_0}{M} \tag{157}$$

In the form for Debye model above, $c_v \to A\ as\ \theta \to \infty$, hence A is the Dulong-Petit limit. There are two unknown constants for a fit to experimental data in the Debye form of specific heat, i.e. A and T_D. The Debye expression is fit to the experimental specific heat data for sucrose assuming $A = 3279 \frac{J}{kg\ K}$ as shown below in Figure 13. It can be noted that since the experimental data for sucrose is available only for a small range of temperatures, it would help to know a more accurate Dulong-Petit Limit (A) for a better prediction at higher temperatures (θ >400K).

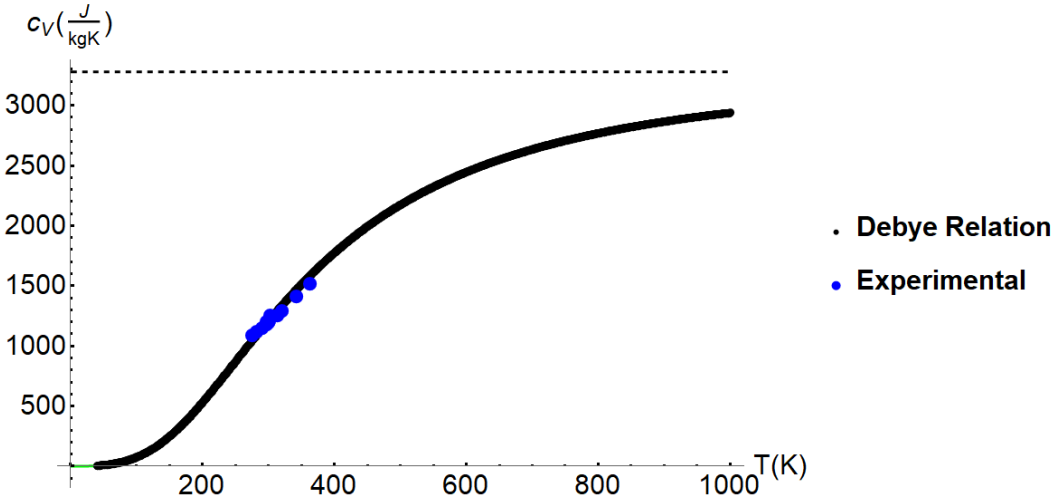

Figure 21. Debye model fit to experimental data for specific heat capacity at constant volume for sucrose

Fitting to an Empirical form : $\widetilde{c_v}(\tilde{\theta}) = \frac{\tilde{\theta}^3}{c_0+c_1\tilde{\theta}+c_2\tilde{\theta}^2+c_3\tilde{\theta}^3}$

In order to provide a simpler expression to calculate the specific heat and enable the integration of the Debye form, the specific heat is fit to an empirical form shown below, as done for HMX by Sewell and Menikoff (*AIP Conference Proceedings*, 157-162, 2004).

$$\widetilde{c_v}(\tilde{\theta}) = \frac{\tilde{\theta}^3}{c_0 + c_1\tilde{\theta} + c_2\tilde{\theta}^2 + c_3\tilde{\theta}^3} \tag{158}$$

where (c_0, c_1, c_2, c_3) are constants. Such a form is chosen as it obeys the asymptotic limits at the two temperature extremes, i.e. $\widetilde{c_v}(\theta) \to \theta^3 \; as \; \theta \to 0$ and $\widetilde{c_v}(\theta) \to \frac{3R_0}{M} = \frac{1}{c_3} as \; \theta \to \infty$ (Dulong-Petit Limit). A fit to the Debye relation for specific heat capacity using the empirical form is shown in Figure 21.

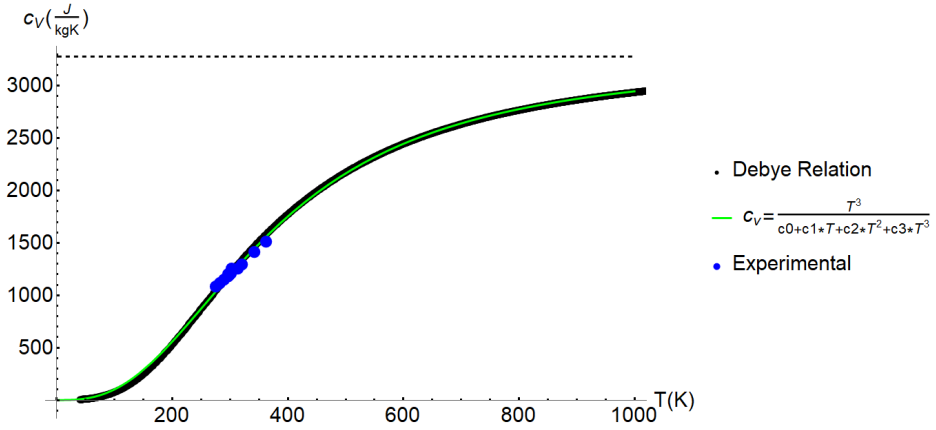

Figure 22. Empirical fit (green line) to Debye model for specific heat of sucrose

It can be seen from the plot above that the empirical relation fits the Debye Model very well. The following set of parameters are used for this fit:

$$c_0 = 7.095 \times 10^3 \frac{kgK^4}{J} \tag{159}$$
$$c_1 = 2.230 \times 10^1 \frac{kgK^3}{J}$$
$$c_2 = 4.180 \times 10^{-3} \frac{kgK^2}{J}$$
$$c_3 = 3.050 \times 10^{-4} \frac{kgK}{J}$$

An explicit expression for the integral of specific heat capacity with temperature is still hard to evaluate using the empirical relation for specific heat. Therefore, the integral is calculated numerically and a quadratic polynomial is fit, as shown in Figure 22. A simple quadratic polynomial is able to fit the data very well.

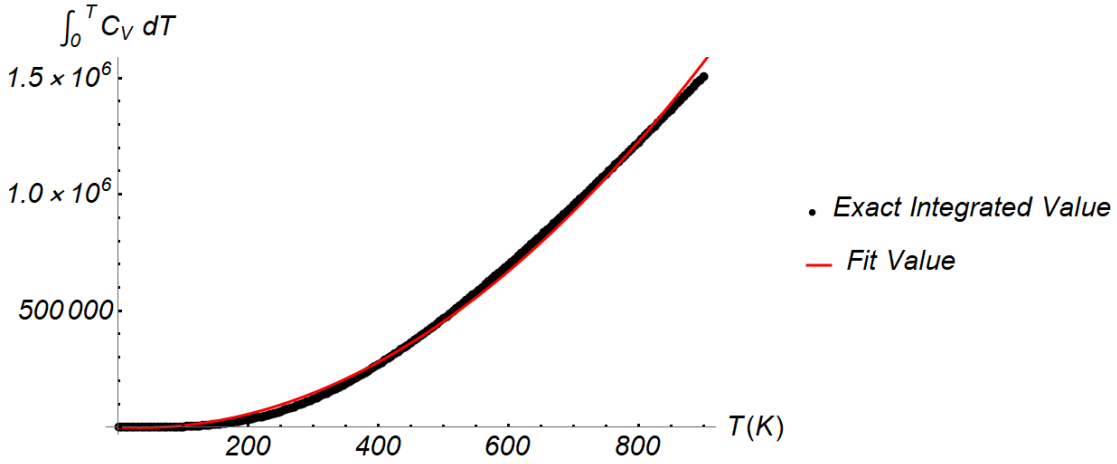

Figure 23. $\int_0^\theta C_v(\theta)d\theta$ is evaluated numerically (thick black curve) and fit to a quadratic function (thin red curve)

Therefore, the approximation is given as: $\int_0^\theta C_v(\theta)d\theta \approx f(\theta) = (-133.647 \times \theta + 2.082 \times \theta^2)\frac{J}{kg}$. So, the complete Mie-Gruneisen EOS (equation (42)) can now be written as:

$$P(v,\theta) = P(V,\theta_0) - \frac{d\phi(v)}{dv} f\left(\frac{\theta}{\phi(v)}\right) \tag{160}$$

Thermal Conductivity

A thermal conductivity value of 0.486 W/m K is reported in Trott et al. (*Journal of Applied Physics,* 101**,** 024917, 2007).

Melting Point/Melt Curve

The melting point temperature of large organic molecules like HMX and sucrose is highly dependent on pressure. Melting is typically described by the Lindemann Law:

$$\theta_m = \theta_{m0} \exp\left[2\Gamma_0(1-\nu) + \frac{2}{3}\ln(\nu)\right] \tag{161}$$

where subscript '0' indicates ambient temperature and pressure. θ_{m0} is the melt temperature, Γ_0 is the Gruneisen parameter, $\nu = \frac{v}{v_0} = \frac{\rho_0}{\rho}$ is the relative volume and ρ represents the density of the solid. Lindemann Law can be linearized as follows:

$$\begin{aligned}\theta_m &= \theta_{m0} \exp\left[2\Gamma_0(1-\nu) + \frac{2}{3}\ln(\nu)\right] \\ &= \theta_{m0} \exp\left[2\Gamma_0 \frac{\Delta v_c}{v_0} + \frac{2}{3}\ln\left(1 - \frac{\Delta v_c}{v_0}\right)\right] \\ &\approx \theta_{m0} \exp\left[2\Gamma_0 \frac{\Delta v_c}{v_0} - \frac{2}{3}\frac{\Delta v_c}{v_0}\right] \\ &= \theta_{m0} + 2\left(\Gamma_0 - \frac{1}{3}\right)\frac{\Delta v_c}{v_0} \\ &= \theta_{m0} + a\frac{\Delta v_c}{v_0}\end{aligned} \tag{162}$$

Δv_c represents compressive change in volume and $a = 2\left(\Gamma_0 - \frac{1}{3}\right)$. This linearized relation is called the Kraut-Kennedy relation. Figure 16 shows a comparison between the Lindemann Law and Kraut-Kennedy relation and the agreement is very close for compressive strain ratios up to 0.2.

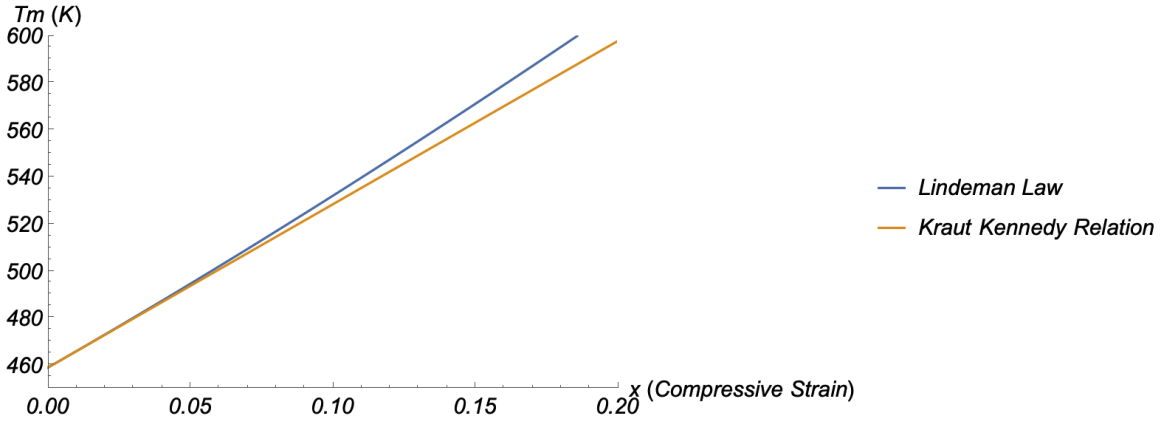

Figure 24. Comparison between Lindemann Law for sucrose and the linearized version (Kraut-Kennedy relation)

Gruneisen parameter

The following functional form of Gruneisen parameter is assumed as noted by Grady, 2017 (*Physics of Shock and Impact, Volume 2:)*:

$$\Gamma(v) = \frac{\Gamma_0}{v_0} v \tag{163}$$

The value of Γ_0 is derived from the following thermodynamic relation to be consistent with values for other thermodynamic quantities:

$$\frac{\Gamma(v)}{v} = \frac{\alpha_v K_T}{c_v} \tag{164}$$

Using the above relations in equations (169) and (170), $\Gamma_0 = 1.09$ is obtained.

The model is implemented in ABAQUS through a VUMAT. Figure 25 shows a preliminary comparison between the experimental results and the model prediction for optimally chosen parameter values. The model predicts that the drop in shear stress is due to formation of an adiabatic shear band within the specimen layer, which is illustrated in Figures 26 and 27.

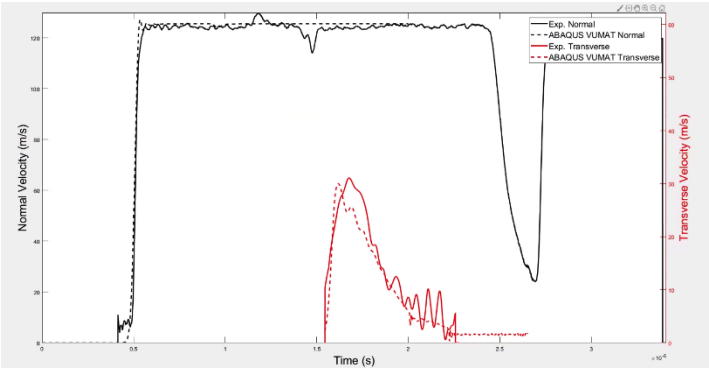

Figure 25. Comparison of the model predictions and the experimental data for sucrose. The solid lines are experimental data and the dashed lines are model fits.

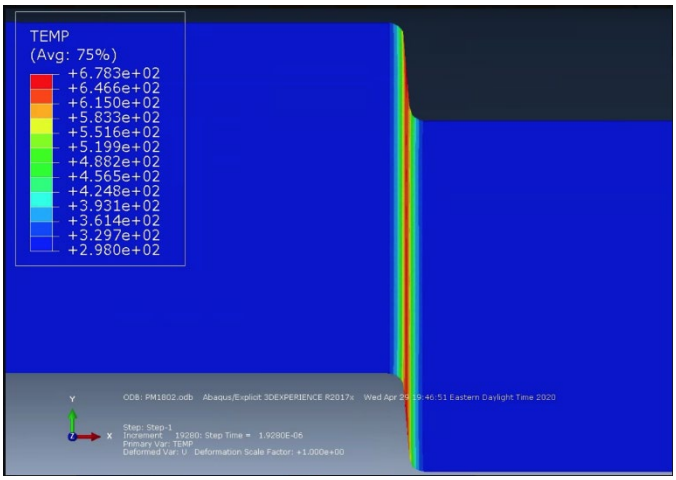

Figure 26.. Computational model of the PSPI experiment with the Johnson-Cook thermoviscoplastic model of sucrose. Note the formation of an adiabatic shear band within the specimen.

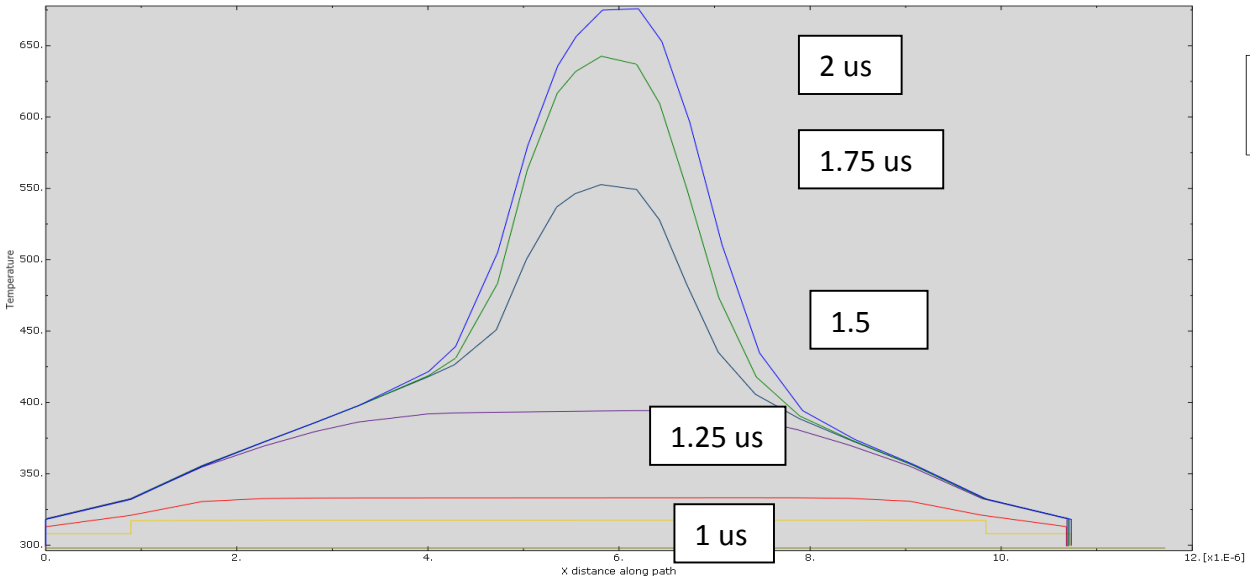

Figure 27. Evolution of the temperature across the specimen thickness as a function of time. Note the formation of the adiabatic shear band, which reduced the strength of the material, which is measured in the PSPI experiment.

6. Development high-speed visible microscopy to characterize the deformation field around individual hot spot events

Dynamic localization and hot spot events in energetic materials occur not only at small time-scales but also at small length-scales, including mechanisms such as adiabatic shear bands, pore collapse, twinning and dynamic friction. Imaging such events requires high temporal and spatial resolutions simultaneously, i.e., *high-speed microscopy*. Here we developed a technique that offers such a capability with a temporal resolution of 250 ns, spatial resolution of ~1 μm and a field of view of about 1.1 mm x 0.63mm. A schematic of the experimental set-up is shown in Fig. 28 and an actual photograph of the setup is shown in Fig. 29. The key components of the high-speed microscopy system are: (a) a high-speed camera, (b) imaging optics and (c) illumination.

A Cordin 560 rotating mirror high-speed camera employed in our setup consists of 78 independent CCD sensors; the mirror can rotate at a speed of up to 16,667 rotations per second, which gives a maximum framing rate of 4 million fps. Each CCD is a monochrome 14-bit sensor with a 1920 x 1080 pixel array and a pixel pitch of 7.4 μm.

The optical imaging system consists of a microscope that forms an image of the specimen surface on a prescribed plane at the entrance of the Cordin camera, from where it is relayed by the internal optics of the camera to the sensor plane via the rotating mirror. The microscope elements are shown in Fig. 28. For illumination, we employ the Specialized Imaging LUX640 pulsed laser source to illuminate the specimen, which is a 400W pulsed laser that emits a low coherence beam at a wavelength of 640 ± 10 nm. It is shown schematically in Figure 28.

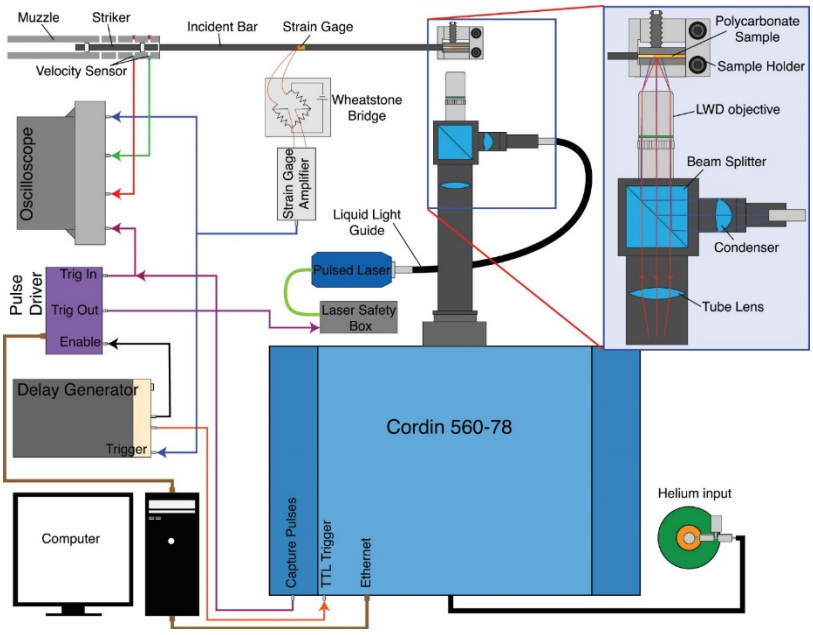

Figure 28. A schematic of high-speed microscope set up for imaging a sample impacted in a Kolsky bar . Key components of the system are: high-speed camera, microscope optics and the laser for illumination.

The capability of the experimental system is demonstrated by imaging the initiation of an adiabatic shear band (ASB) from a notch tip in a polycarbonate specimen subjected to impact loading in a Kolsky bar. A pre-crack is made in the polycarbonate sample at the tip of the machined notch using a sharp razor. The deformation field is measured through particle tracking by depositing a grid of 10 μm sized circular copper dots, with a pitch of 20 μm in both directions (Fig. 30). Figure 31 shows a sequence of high-speed micrographs of the deformation field near the crack tip. Fig 32 shows contours of the corresponding Lagrangean shear strain. Localization of deformation into an adiabatic shear band is visualized by selecting a vertical line ahead of the crack tip and plotting the x-displacement and the shear strain along the line as a function of time, as shown in Fig 33. It should be noted that since all measurements reported here are kinematic in nature, the discussion is limited to kinematic signatures of the onset of the localization/instability. More definitive conclusions will have to await the calculation of the stress field and the shear traction on the crack plane from the measured kinematic fields.

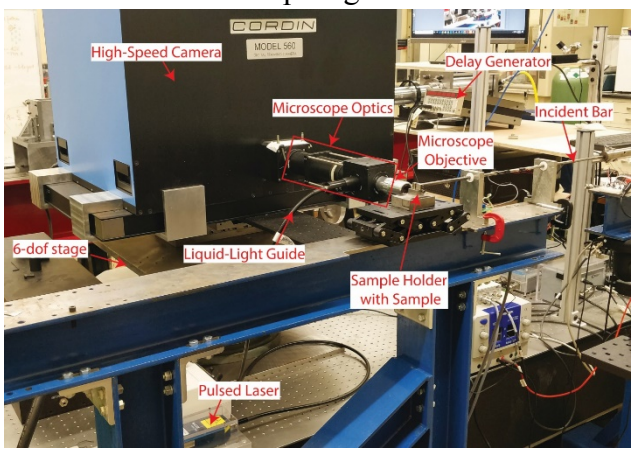

Figure 29.High-speed microscope set-up at Brown University.

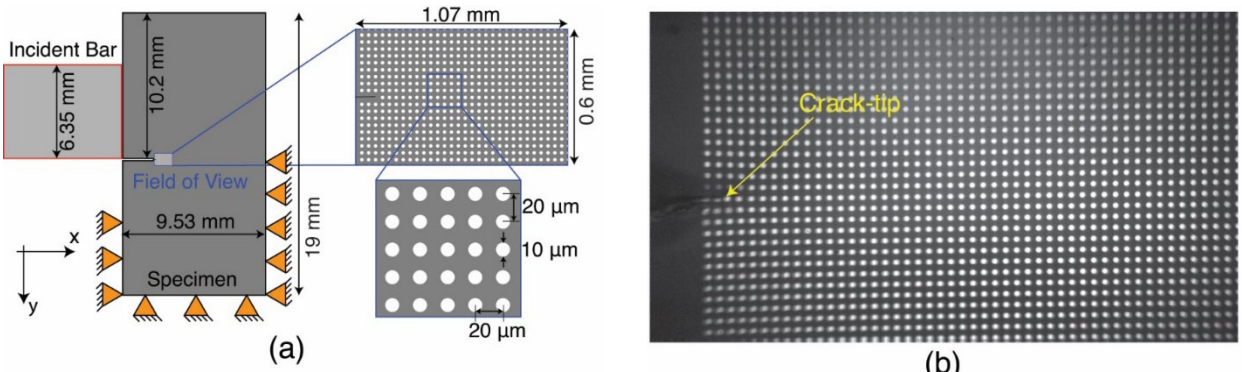

Fig. 30 (a) Edge-on impact on the polycarbonate specimen. The specimen is fixed on the bottom half at the back to prevent rigid translation. Fixing on the bottom face and bottom half of the front face impedes rigid rotation. Lateral confinement (not shown here) is provided on either side of the specimen plate to minimize out of plane motion. The field of view with a 20x objective is shown. 10 μmsized Cu dots, spaced 20 μm apart are used for particle tracking. (b) High-speed camera image of the specimen before the arrival of longitudinal compressive wave at the crack tip

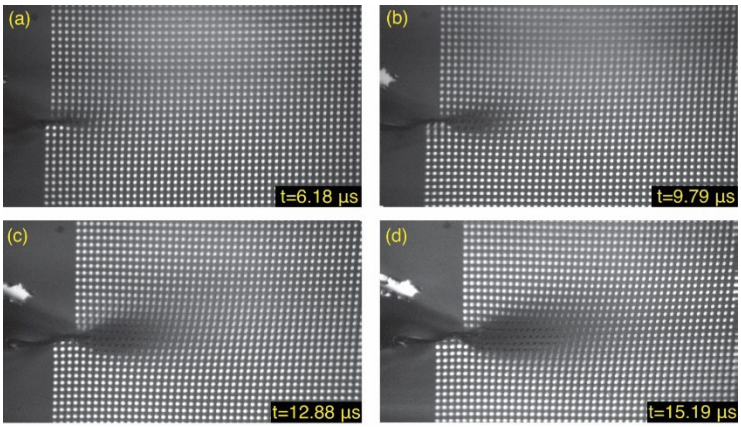

Fig. 31 As acquired images of the notched polycarbonate plate undergoing deformation taken at different time instants: (a) t=6.18 μs, (b) t=9.79 μs, (c) t=12.88 μs, (d) t=15.19 μs.

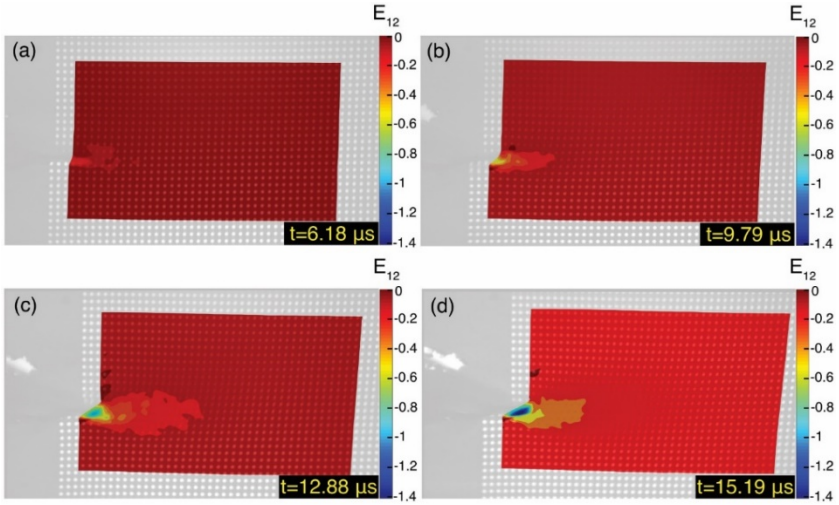

Fig. 32. Lagrangian shear strain, E_{12} plotted at (a) t=6.18 μs, (b) t=9.79 μs, (c) t=12.88 μs and (d) t=15.19 μs

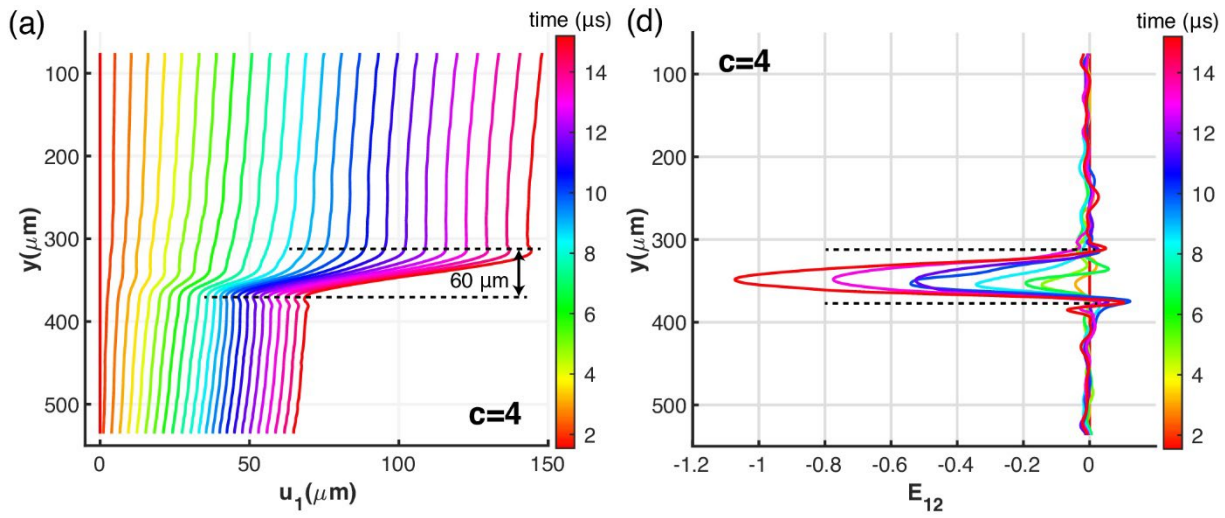

Figure 33. Evolution of x-displacement, u_1 and the corresponding Lagrangian shear strain, E_{12} slightly ahead of the crack tip, showing initiation of an adiabatic shear band, the width of which is approximately 50 μm.

SUMMARY

- PSPI experiments have been conducted on HTPB binder, sucrose simulant and their composite.
- Constitutive models have been developed for HTPB and sucrose. For the latter, the fall in shear strength is predicted to be through the formation of an adiabatic shear band.
- The constitutive models developed for HTPB and sucrose are being used to simulate the PSPI experiments on the composite and reveal the deformation mechanisms.
- We have developed a high-speed microscopy technique to image the deformation field near individual hot spot events.

References

1. J. L. Jordan, D. Montaigne, P. Gould, C. Neel, G. Sunny and C. Molek, Journal of Dynamic Behavior of Materials **2**, 91-100 (2016).
2. C. M. Cady, W.R. Blumenthal and G.T. Gray III, Polymer Engineering and Science, **46(6)**, 812-819 (2006).
3. C. R. Siviour, P.R. Laity, W.G. Proud, J.E. Field, D. Porter, P.D. Church, P. Gould and W.H. Thresher, Proceedings of the Royal Society A, **464(2093)**, 1229-1255 (2008).
4. J. C. F. Millett, N. K. Bourne and J. Akhavan, Journal of Applied Physics, **95(9)**, 4722-4727 (2004).
5. S. A. Sheffiedl, R. L. Gustavsen and R. R. Alcon," Porous HMX Initiation Studies-Sugar as an Inert Simulant," Shock Compression of Condensed Matter, p.575 (1997).
6. J. C. F. Millett and N. K. Bourne, Journal of Physics D, **37**, 2613-2617 (2004).
7. S. N. Heavens and J. E. Field, Proceedings of the Royal Society of London A, **338**, 77-93 (1974).

8. R. J. Clifton and R. W. Klopp, *Metals Handbook 9th Edition*, American Society for Metals, Vol. 8, Metals Park, OH, 1985, pp. 230-239.
9. C. Williams, S. Walker, I. Lochert and S. Clarke, New Trends in Research of Energetic Materials, 398-405 (2013).
10. A. V. Shastry and R. W. Hartel, Journal of Food Engineering, **30**, 75-94 (1996).
11. D. Porter, *Group interaction modelling of polymer properties,* CRC Press, New York, (1995)